J. Fluid Mech. (1994), *vol.* 267, *pp.* 221–250

Wind effects on the nonlinear evolution of slowly varying gravity–capillary waves

By TETSU HARA[1] AND CHIANG C. MEI[2]

[1] Graduate School of Oceanography, University of Rhode Island, Narragansett, RI 02882, USA

[2] Department of Civil and Environmental Engineering, Massachusetts Institute of Technology, Cambridge, MA 02139, USA

(Received 21 December 1992 and in revised form 26 October 1993)

A train of uniform two-dimensional gravity waves in deep water is known to be unstable to certain sideband disturbances. If the time of propagation is sufficiently long for the fourth-order terms to be important, the sidebands may grow at unequal rates, resulting in a downward shift of peak frequency. But this shift is only a temporary phase of a recurrent evolution process. Recent work by us (Hara & Mei 1991) has shown that wind and dissipation can help maintain this downshift at large time. In this paper we examine a similar two-dimensional problem for capillary–gravity waves. The basic flow in air and water is assumed to be steady, horizontally uniform and turbulent; the wave-induced flow in both media is assumed to be laminar. Evolution equations are deduced with wind and dissipation included in such a way that their influence is comparable to the asymmetric spectral evolution. After finding the initial growth rates of unstable sidebands, the nonlinear development of modulational instability is examined by integrating the evolution equations numerically. Computed results show that persistent downshift of frequency can happen for relatively long waves, but upshift occurs for very short waves.

1. Introduction

Gravity–capillary waves are known to play an important role in the initial stage of wind-wave generation. Recent advances in satellite remote sensing have spurred intensive interest in the dynamics of gravity–capillary waves since they are responsible for the Bragg scattering of short radar signals. A complete account of the evolution of the gravity–capillary wave spectrum is however complicated since it must involve wave–wave interaction, energy and momentum transfer from the wind, and possibly wave breaking. The last aspect cannot yet be treated by existing theoretical means. While the first two factors have been investigated separately, understanding of their combined effects is wanting.

In the gravity–capillary range, wave–wave interaction is possible among three distinctive wavenumbers (McGoldrick 1965). However, for relatively long gravity–capillary waves four-wave interaction can be significant, which includes as a special case the problem of sideband instability. The nonlinear envelope equation and the linearized instability of side bands for gravity–capillary waves were first obtained by Djordjevic & Redekopp (1977) up to third order of wave steepness. Extension to the fourth order in the manner of Dysthe (1979) was made by Hogan (1985) for deep water, who also performed the linear instability analysis. Calculations of the nonlinear evolution of the unstable sidebands have apparently not yet been reported in the literature.

Studies of the wind generation of gravity–capillary waves have been mainly focused on the initial stage of unstable growth. In his linearized analysis of instability, Miles (1961) solved the Orr–Sommerfeld equation for the wave-induced disturbances in air for a linear-logarithmic wind profile. His theory was extended by Valenzuela (1976) for a coupled air–water system. Laboratory measurements of wave growth rate were conducted by Larson & Wright (1975) who observed broad-banded wind-generated waves. Kawai (1979) studied the generation of initial wavelets both theoretically and experimentally. His calculations of the wavenumber and the growth rate of the most unstable mode agreed well with measured values. It has also been noted that after the initial wavelets attain certain magnitude, the peak of the wave spectrum begins to migrate to lower frequency while the wave surface pattern becomes more irregular. A similar phenomenon of frequency downshift is known to exist in surface gravity waves. Van Gastel, Janssen & Komen (1985) also examined the initial growth rate of gravity–capillary waves using various shear models; they found that the growth rate can be very sensitive to the wind profile assumed, whereas the wind-induced current profile in water has much less influence.

A nonlinear theory motivated by wind effects over waves has been given by Blennerhassett (1980), who derived the nonlinear evolution equation of interfacial waves between two viscous fluids bounded by two horizontal plates moving horizontally. Janssen (1986) studied the period-doubling of wind-induced gravity–capillary waves first observed by Choi (1977). Expanding an earlier work of Chen & Saffman (1979), he examined the effects of wind on Wilton's ripples due to second-harmonic resonance. He incorporated a wind-energy input coefficient and assumed linear shear in water in the evolution equations which couple the first and second harmonics. Numerical calculations of the nonlinear evolution indeed gives rise to a rapid period doubling. This mechanism is however important only near a particular frequency (19.6 Hz); a more general theory for different frequencies which includes both wave/wave interaction and wind effect is desirable.

For deep-water gravity waves the nonlinear mechanics of Benjamin–Feir instability has been studied extensively without wind. By integrating numerically the nonlinear Schrödinger equation, Lake *et al.* (1977) found that the upper and lower sidebands first grow at equal rates, at the expense of the carrier wave. Afterwards the carrier wave and the sidebands exchange energy cyclically. Extension of the Schrödinger equation to the fourth order in wave steepness was made by Dysthe (1979), based on which Lo & Mei (1985) re-examined the nonlinear evolution of side-band instability. While the lower sideband was found to grow faster than the upper sideband in the initial stage, subsequent evolution still shows a recurrence pattern. Therefore the peak frequency downshift is only temporary near the peaks of modulation. By incorporating heuristically an empirical model for breaking waves into Dysthe's extended equation, Trulsen & Dysthe (1989) showed more persistent frequency downshift. Recently the present authors (Hara & Mei 1991) have extended the work of Lo & Mei by including the effect of wind input and internal dissipation. The long-time evolution of the sideband instability demonstrates that permanent downshift of peak frequency is possible without breaking.

In this study, we shall examine whether wind and viscous dissipation may enhance persistent frequency shift in gravity–capillary waves. For simplicity the waves are assumed to be two-dimensional and narrow banded. While the basic wind and water current are assumed to have linear-logarithmic profiles, the wave-induced disturbance is assumed to be laminar, because of the very short wavelength. We also assume that the rates of energy input from wind and viscous dissipation are comparable to the rate

of asymmetric spectral growth. This assumption of course imposes constraints on the wind speed and the wave steepness, hence on the range of applicability of the theory.

After presenting the basic formulation in §2, the air flow over gravity–capillary waves is examined in §3. In particular the wind-energy input is calculated to be a nonlinear function of the wave steepness. The nonlinear evolution equation of the wave amplitude is then derived in §4, including the effects of wind, wind-induced water current, and viscosity. The initial growth rate and the subsequent nonlinear evolution of Benjamin–Feir instability are examined in §§5 and 6 respectively for three different wavelengths. Since the mathematical procedure is very close to that for gravity waves in Hara & Mei (1991), we present the basic formulation and the numerical procedure briefly and focus on the results, which are different from the gravity wave case.

2. Formulation for the basic flow and wave disturbances

Since the following analysis is very similar to the case of gravity waves, we briefly summarize the basic equations and assumptions. Complete derivations are given in Hara & Mei (1991) and are not repeated here.

We first introduce the normalization in terms of the characteristic wavenumber of the free surface k, the acceleration due to gravity g, and the density of air ρ' or of water ρ. All the equations in the following discussion are dimensionless unless stated otherwise. All quantities associated with air are distinguished by primes. Let (x, y) be a Cartesian coordinate system with x in the common direction of the wind and the wave propagation, and y in the upward vertical direction. The basic wind in air (distinguished by the superscript b) in the absence of waves is assumed to be of a linear-logarithmic profile, described by

$$u'^b = s'y, \qquad y < \delta'_v = 5(\sigma'^2/s')^{\frac{1}{2}}$$

$$= s'\left[5(\sigma'^2/s')^{\frac{1}{2}} + \frac{1}{\kappa}(\sigma'^2/s')^{\frac{1}{2}}(\alpha' - \tanh\tfrac{1}{2}\alpha')\right], \quad y > \delta'_v, \tag{2.1}$$

with

$$\sinh\alpha' = 2\kappa(s'/\sigma'^2)^{\frac{1}{2}}(y - 5(\sigma'^2/s')^{\frac{1}{2}}), \tag{2.2}$$

where $\kappa = 0.4$ is the Kármán constant, $\sigma'^2 = \nu'(k^3/g)^{\frac{1}{2}}$ is the viscosity parameter, δ'_v is the dimensionless thickness of the air viscous sublayer, $s' = u'^2_*/\nu'(gk)^{\frac{1}{2}}$ is the normalized wind shear, ν' is the kinematic viscosity, and u'_* is the friction velocity. The same wind profile has been used by Miles (1957) and Kawai (1979) for the analysis of the initial growth of gravity–capillary waves. The normalized basic current in water is also assumed to be of the same form, and is obtained by removing the primes and changing the signs of u^b and y in (2.1) and (2.2).

The wave-induced disturbances u', v' (the velocities in the x, y-directions) and p' (the dynamic pressure) in air are assumed to be governed by laminar Navier–Stokes equations:

$$\frac{\partial u'}{\partial x} + \frac{\partial v'}{\partial y} = 0, \tag{2.3}$$

$$\frac{\partial u'}{\partial t} + (u' + u'^b)\frac{\partial u'}{\partial x} + v'\frac{\partial (u' + u'^b)}{\partial y} = -\frac{\partial p'}{\partial x} + \sigma'^2\nabla^2 u', \tag{2.4}$$

$$\frac{\partial v'}{\partial t} + (u' + u'^b)\frac{\partial v'}{\partial x} + v'\frac{\partial v'}{\partial y} = -\frac{\partial p'}{\partial y} + \sigma'^2\nabla^2 v', \tag{2.5}$$

$$\nabla^2 = \frac{\partial^2}{\partial x^2} + \frac{\partial^2}{\partial y^2}. \tag{2.6}$$

The governing equations for wave-induced disturbances in water are obtained from (2.3)–(2.6) by dropping the primes.

It is in principle possible to include the effect of air turbulence in a more direct manner, such as using a turbulence closure model. However, since the purpose of this study is not to examine the detailed structure of the modulated air flow over waves, but to examine the effect of wind energy input on the nonlinear evolution of water waves, we adopt this simple model here.

On the interface $y = \zeta(x, t)$, the kinematic boundary conditions are

$$\frac{\partial \zeta}{\partial t} + (u + u^b)\frac{\partial \zeta}{\partial x} - v = \frac{\partial \zeta}{\partial t} + (u' + u'^b)\frac{\partial \zeta}{\partial x} - v' = 0, \quad y = \zeta \tag{2.7}$$

and

$$u + u^b = u' + u'^b, \quad v = v', \quad y = \zeta. \tag{2.8}$$

We further require that the tangential derivative of the normal stress is continuous across the air–water interface:

$$\left(\frac{\partial u}{\partial t} + u\frac{\partial u}{\partial x} + v\frac{\partial u}{\partial y} - \sigma^2\nabla^2 u\right) + \left(\frac{\partial v}{\partial t} + u\frac{\partial v}{\partial x} + v\frac{\partial v}{\partial y} - \sigma^2\nabla^2 v\right)\frac{\partial \zeta}{\partial x}$$
$$+ \frac{\partial \zeta}{\partial x} + \sigma^2\left(\frac{\partial}{\partial x} + \frac{\partial \zeta}{\partial x}\frac{\partial}{\partial y}\right)\left[2\frac{\partial u}{\partial x}n_x n_x + 2\frac{\partial v}{\partial y}n_y n_y + 2\left(\frac{\partial u}{\partial y} + \frac{\partial v}{\partial x}\right)n_x n_y\right]$$
$$- \gamma\frac{\partial}{\partial x}\left\{\frac{\partial^2 \zeta}{\partial x^2}\left[1 + \left(\frac{\partial \zeta}{\partial x}\right)^2\right]^{-\frac{3}{2}}\right\}$$
$$= \frac{\rho'}{\rho}\left(\gamma\frac{\partial^3 \zeta}{\partial x^3} - \sigma'^2\frac{\partial^2 u'}{\partial y^2}\right)[1 + O(\epsilon, \delta'^2)] \equiv \frac{\partial f_b'}{\partial x}, \quad y = \zeta, \tag{2.9}$$

where f_b' denotes the normal stress due to wind, ϵ is the typical wave steepness, and δ' is the dimensionless air boundary-layer thickness to be examined in §3. Similarly the continuity of the tangential stress yields

$$\sigma^2\left[2\frac{\partial u}{\partial x}n_x n_y + \left(\frac{\partial u}{\partial y} + \frac{\partial v}{\partial x}\right)(n_y n_y - n_x n_x) - 2\frac{\partial v}{\partial y}n_x n_y\right]$$
$$= \frac{\rho'\sigma'^2}{\rho}\frac{\partial u'}{\partial y}[1 + O(\epsilon, \delta'^2)] \equiv f_a', \quad y = \zeta, \tag{2.10}$$

where f_a' denotes the tangential stress due to wind. The surface tension between air and water Γ has been normalized by

$$\gamma = \Gamma k^2/\rho g, \tag{2.11}$$

and

$$\frac{1}{R} = \frac{\partial^2 \zeta}{\partial x^2}\left[1 + \left(\frac{\partial \zeta}{\partial x}\right)^2\right]^{-\frac{3}{2}} \tag{2.12}$$

is the inverse of the radius of curvature of the free surface. The components n_x, n_y are of the unit vector normal to the water surface.

In view of the much smaller lengthscale, we assume the disturbances due to gravity–capillary waves to be laminar. Therefore the constant eddy viscosity used in Hara & Mei (1991) is replaced by the kinematic viscosity. Apart from this and the inclusion of capillarity, the formulation here remains identical to our previous paper.

k/k_c	γ	σ^2	σ'^2
0.2	0.04	2.00×10^{-4}	3.01×10^{-3}
0.3	0.09	3.68×10^{-4}	5.52×10^{-3}
0.9	0.81	1.91×10^{-3}	2.87×10^{-2}

TABLE 1. Values of parameters $\gamma, \sigma^2, \sigma'^2$

A reference wavenumber k_c, which corresponds to the linear waves with minimum phase speed, may be defined by

$$k_c^2 = \rho g/\Gamma \quad \text{so that} \quad \gamma = (k/k_c)^2. \tag{2.13}$$

For the following typical values at 20 °C:

$$\left.\begin{aligned} \rho = 0.998\ \text{g cm}^{-3}, \quad \rho' = 0.00121\ \text{g cm}^{-3}, \quad g = 980\ \text{cm s}^{-2}, \\ \nu = 0.0100\ \text{cm}^2\ \text{s}^{-1}, \quad \nu' = 0.150\ \text{cm}^2\ \text{s}^{-1}, \quad \Gamma = 72.8\ \text{g s}^{-2} \end{aligned}\right\} \tag{2.14}$$

the value of k_c is

$$k_c = 3.67\ \text{cm}^{-1}. \tag{2.15}$$

In table 1 γ, σ^2 and σ'^2 are evaluated for $k/k_c = 0.2$, 0.3 and 0.9.

Throughout this paper, the typical wave steepness ϵ is assumed to be small. This parameter is assumed to characterize the slowness of the amplitude modulation as well, so as to achieve a balance between nonlinearity and dispersion. Our analysis focuses on the circumstance where the wave growth due to wind and the viscous dissipation in water are comparable with the effect of asymmetry of sideband instability, which is known to occur over $t = O(1/\epsilon^3)$. Therefore we set

$$\sigma^2 \equiv N\epsilon^3, \tag{2.16}$$

where N is a constant of $O(1)$. This in turn imposes a constraint on the wave steepness ϵ, since the viscosity parameter σ^2 is a fixed small number for a given relative wavenumber k/k_c in table 1. We shall also choose the wind strength so that the wind input is comparable with the viscous dissipation, i.e. so that the right-hand side of (2.9) is of $O(\epsilon^4)$. Although these assumptions limit the range of the wave steepness and the wind strength, we believe that the analysis of nearly neutral conditions is an important first step toward a better understanding of the subtle interplay among nonlinearity, dispersion, and energy input/output.

Our basic formulation closely resembles that by Blennerhassett (1980). While he has subsequently analysed the third-order nonlinear evolution of a coupled air–water system, we decouple the air and the water problems by using the fact that the density of air is much smaller than that of water. This decoupling significantly simplifies the mathematical procedures, and enables us to examine the fourth-order nonlinear effects necessary for non-recurrent and asymmetric evolution in the nonlinear stage.

3. Air flow over gravity–capillary waves

3.1. *Reduction of the boundary value problem*

Since the effect of air flow (surface stresses) on the evolution of surface waves is assumed to be important only at the highest order in wave steepness ϵ, one needs to solve for the air flow only to the leading order. The kinematic boundary conditions for air at the interface are first determined from the leading-order wave motion in water.

On the other hand the basic drift current due to air flow over a plane free surface without waves is $u^b = O[(s\sigma^2)^{\frac{1}{3}}\ln(s/\sigma^2)^{\frac{1}{3}}]$, which can be kept at $O(\epsilon)$ or less for certain range of wind intensity, as will be shown later. Therefore it has a negligible effect on the water wave to the leading order.

Let the wave profile be given, to the leading order, by

$$\zeta = \epsilon\tfrac{1}{2}A\,\mathrm{e}^{\mathrm{i}(x-ct)} + *, \tag{3.1}$$

where the asterisk denotes higher-order terms, and where the normalized dispersion relation is

$$c^2 = 1+\gamma = 1+(k/k_c)^2. \tag{3.2}$$

The complex wave amplitude A is expected to be a function of long scales, and is written as

$$A = B\mathrm{e}^{\mathrm{i}D}, \tag{3.3}$$

where $B = O(1)$ and D are the absolute amplitude and phase. The absolute amplitude B is related to the dimensional wave amplitude a by $\epsilon B = ka$. It is now convenient to introduce orthogonal curvilinear coordinates ξ', η defined by

$$x-ct+D = \xi' - \epsilon B\sin\xi'\,\mathrm{e}^{-\eta}, \quad y = \eta+\epsilon B\cos\xi'\,\mathrm{e}^{-\eta}. \tag{3.4a, b}$$

In this moving coordinate system the wave surface is flat, $\eta = 0$, up to $O(\epsilon)$; this is accurate enough in order to solve the air flow to the leading order in ϵ. Let us define the stream function ψ'^b of the basic flow and ψ' of the wave-induced flow in air by

$$\frac{\partial\psi'^b}{\partial y} = u'^b, \quad \frac{\partial\psi'}{\partial y} = u', \quad -\frac{\partial\psi'}{\partial x'} = v'. \tag{3.5}$$

The governing equation for ψ' then becomes,

$$-\frac{\partial(\psi'^b - cy, \nabla'^2\psi')}{\partial(\xi',\eta)} - \frac{\partial(\psi'[\partial^2\psi'^b/\partial y^2])}{\partial(\xi',\eta)} - \frac{\partial(\psi', \nabla'^2\psi')}{\partial(\xi',\eta)} = \sigma'^2\nabla'^2\nabla'^2\psi', \tag{3.6}$$

where the Jacobian of transformation has been approximated by 1 to the leading order. It can be shown (Hara & Mei 1991) that the nonlinear term (the third term) is significant even at the leading order. Consequently the surface stresses due to wind can depend explicitly on the wave steepness ϵB, and differ from Janssen's (1986) model of constant energy input rate. In the first term $-cy$ appears because of the shift of coordinate. The boundary conditions at the interface are derived from the orbital motion of the leading-order water waves:

$$\frac{\partial\psi'}{\partial\xi'} = -\frac{\partial\psi'^b}{\partial\xi'} - \epsilon cB\sin\xi', \quad \frac{\partial\psi'}{\partial\eta} = -\frac{\partial\psi'^b}{\partial\eta} + \epsilon cB\cos\xi', \quad \eta = 0. \tag{3.7}$$

For the air flow far above, the wavy water surface is expected to increase the effective roughness. Therefore for a fixed wind stress, the wind speed decreases by a constant. This is due to a mechanism analogous to induced streaming outside an oscillatory boundary layer. We therefore impose the following boundary conditions:

$$\frac{\partial\psi'}{\partial\eta} = \text{const.}, \quad \frac{\partial\psi'}{\partial\xi'} = 0, \quad \eta = \infty. \tag{3.8a, b}$$

The constant in (3.8a), which corresponds to the decrease in wind speed, is to be found from the numerical solution.

In (2.1) and (3.6)–(3.8), there are four dimensionless parameters: the wind shear s', the phase velocity c, the viscosity parameter σ', and the wave slope $\epsilon B = ka$. The first three parameters may be rewritten in terms of the relative wavenumber k/k_c, the normalized friction velocity $u'_*/\nu' k_c$, and a non-dimensional quantity $\sigma'_c \equiv \nu'(k_c^3/g)^{\frac{1}{3}}$ which is a property of the fluid. Therefore the air flow depends only on the three controlling parameters k/k_c, $u'_*/\nu' k_c$, and ϵB.

3.2. *Method of solution*

The boundary value problem is solved numerically by the spectral method (Caponi *et al.* 1982). The Fourier expansion

$$\psi' = \epsilon B \sum_{n=-\infty}^{\infty} f_n(\eta)\, \mathrm{e}^{\mathrm{i}n\xi'} \tag{3.9}$$

is introduced into the governing equation and the boundary conditions. The resulting coupled nonlinear ordinary differential equations are solved by finite differences. Details are given in Hara (1990).

The result is then introduced to (2.9) to calculate the variation of the normal wind stress on the water surface:

$$\frac{\partial f'_b}{\partial x} \approx \frac{\rho'}{\rho}\left[\epsilon\gamma\left(A\frac{1}{2\mathrm{i}}\mathrm{e}^{\mathrm{i}(x-ct)} + *\right) - \sigma'^2 \epsilon B \sum_{n=-\infty}^{\infty}\left(\frac{\partial^3 f_n}{\partial \eta^3}\right)_{\eta=0} \mathrm{e}^{\mathrm{i}n(x-ct)}\, \mathrm{e}^{\mathrm{i}nD}\right]. \tag{3.10}$$

Since the wind strength s' is chosen so that (3.10) is $O(\epsilon^4)$, we let

$$\frac{\partial f'_b}{\partial x} = N\epsilon^4 \sum_{n=-\infty}^{\infty} p_n\, \mathrm{e}^{\mathrm{i}n(x-ct)}. \tag{3.11}$$

Of particular interest is the coefficient of the first harmonic

$$p_1 = A\frac{\rho'}{\rho}\frac{1}{\sigma^2}\left[\frac{\gamma}{2\mathrm{i}} - \sigma'^2\left(\frac{\partial^3 f_1}{\partial \eta^3}\right)_{\eta=0}\right] = O(1), \tag{3.12}$$

which is responsible for the growth and the phase shift of the wave amplitude A. Similarly the tangential stress defined by (2.10) can be calculated:

$$f'_a \approx \frac{\rho'\sigma'^2 \epsilon B}{\rho} \sum_{n=-\infty}^{\infty}\left(\frac{\partial^2 f_n}{\partial \eta^2}\right)_{\eta=0} \mathrm{e}^{\mathrm{i}n(x-ct)}\, \mathrm{e}^{\mathrm{i}nD}, \tag{3.13}$$

which is also formally rewritten as

$$f'_a = N\epsilon^4 \sum_{n=-\infty}^{\infty} q_n\, \mathrm{e}^{\mathrm{i}n(x-ct)}, \tag{3.14}$$

where the first harmonic q_1 is of $O(\delta')$. Since the zeroth harmonic q_0 is the result of nonlinearity in the governing equation (3.6), its magnitude can be estimated to be no greater than $O(\epsilon)$. The mean tangential stress q_0 affects the phase and group velocities of surface waves.

3.3. *Rate of energy transfer*

The energy input rate from air to water through the normal stress is obtained by taking the time average of the product of the first harmonic of the normal stress f'_b and the vertical orbital velocity v at the interface. The contribution from the tangential stress

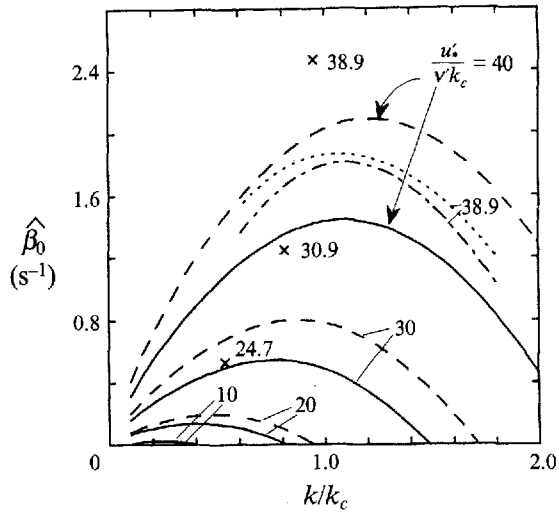

FIGURE 1. Linear dimensional growth rate $\hat{\beta}_0$ against relative wavenumber k/k_c. The numbers indicate normalized friction velocity $u'_*/\nu' k_c$. ——, Calculated from normal stress only; —, calculated from both normal and tangential stresses; ×, experiment by Kawai (1979); · · · · ·, calculation by Kawai (1979); –·–, calculation by van Gastel *et al.* (1985).

is smaller by $O(\delta')$ and is neglected. The growth rate $\tilde{\beta}^r$ of the wave energy due to wind and the corresponding imaginary part $\tilde{\beta}^i$ are then calculated to be

$$\tilde{\beta}^r = 2\frac{\sigma^2}{c}\mathrm{Re}\left(\frac{p_1}{A}\right), \quad \tilde{\beta}^i = 2\frac{\sigma^2}{c}\mathrm{Im}\left(\frac{p_1}{A}\right), \tag{3.15}$$

where the latter is responsible for the phase shift of surface waves. The net growth rate is obtained by subtracting the well-known viscous dissipation rate in water:

$$\tilde{\beta} = \tilde{\beta}^r - 4\sigma^2 = \sigma^2\left[\frac{2}{c}\mathrm{Re}\left(\frac{p_1}{A}\right) - 4\right]. \tag{3.16}$$

The initial growth rate is the limit of zero amplitude, and is given, in dimensional form, as

$$\hat{\beta}_0 = \nu k^2\left[\frac{2}{c}\mathrm{Re}\left(\frac{p_1}{A}\right)_{|A|=0} - 4\right]. \tag{3.17}$$

We shall now compare our numerical results of initial growth rate with earlier works by Kawai (1979) and van Gastel *et al.* (1985). Kawai measured the growth rate of initial wavelets experimentally, and compared it with numerical predictions based on the linearized Orr–Sommerfeld equation. Van Gastel *et al.* gave an asymptotic solution to a similar Orr–Sommerfeld equation, after neglecting the contribution of the tangential surface stress. In both papers it has been shown that the growth rate changes significantly for different wind profiles in air, but it is relatively insensitive to the drift current profiles.

In figure 1 the dimensional linear growth rate $\hat{\beta}_0$ is plotted against the relative wavenumber k/k_c for various values of normalized friction velocity $u'_*/\nu' k_c$. For comparison we also plot the numerical results of Kawai (dotted line) and van Gastel *et al.* (dot-dash line) for $u'_*/\nu' k_c \approx 38.9$, and experimental results of Kawai for three different wind strengths (crosses). Our result for the very strong wind with $u'_*/\nu' k_c =$

k/k_c	$\frac{u'_*}{\nu' k_c}$	s'	s	$(s\sigma^2)^{\frac{1}{2}} \ln (s/\sigma^2)^{\frac{1}{2}}$
0.2	10	7.52	0.137	0.0171
0.3	10	6.14	0.112	0.0184
0.3	12	8.83	0.161	0.0234
0.9	22	17.2	0.312	0.0622

TABLE 2. Selected values of normalized friction velocity, shear rates and measure of water current

40 (solid line) is somewhat smaller than the numerical results by others. However, we have found that for relatively stronger wind or shorter waves, the second derivative of the perturbed air stream function $\partial^2 f_1/\partial\eta^2$, which is the measure of the tangential stress, is maximum at the wave surface, while the third derivative $\partial^3 f_1/\partial\eta^3$ (measure of the normal stress) attains its maximum away from the surface. As a result the ratio of the tangential stress to the normal stress on the surface is numerically larger than the theoretical prediction of $O(\delta')$. In figure 1 the initial growth rate including the effect of tangential stress is also plotted by dashed lines; the agreement with other results is improved. We have also found similar agreement at different wind speeds (Hara 1990). The experimental results by Kawai are always larger than numerical values by us or others. The agreement can be improved if the thickness of the air viscous sublayer δ'_v is increased (Kawai 1979). However, we will not pursue other values of δ'_v in this study. In the following analysis of sideband instability we shall only examine cases where the wind is relatively weak; the tangential stress is less effective and therefore neglected in the calculation of growth rate.

Since we are interested in the very slow evolution, the wind intensities will be selected such that the net growth rate is sufficiently small. Referring to figure 1, the points of intersection of the growth curves and the horizontal axis give the wind strength of no net growth for a given wavenumber. Guided by these curves several wind intensities have been chosen for three wavenumbers to be used later in §6, as listed in table 2. The corresponding shear rates s', s, and the measure of the water current $(s\sigma^2)^{\frac{1}{2}} \ln (s/\sigma^2)^{\frac{1}{2}}$ are also tabulated.

Note that for the chosen wind intensities, the wind shear s' in air is always much larger than 1. On the other hand the values of the measure of the water current in the last column are reasonably small as assumed at the beginning of §3.1. The normalized air boundary-layer thickness δ' can also be estimated from the values in tables 1 and 2 to be in range of 0.05–0.12, which is indeed small.

In figure 2 the nonlinear growth rate $\tilde{\beta}^r$ and the viscous dissipation rate are plotted for a wide range of wave slope $\epsilon B = ka$. The imaginary part of the wind forcing $\tilde{\beta}^i$ is also shown. The growth rate can decrease significantly as the wave steepness increases for longer waves ($k/k_c = 0.2, 0.3$), though not for shorter waves ($k/k_c = 0.9$).

We now present some calculated streamlines of the air flow above the water surface. Figure 3 gives the stream-function contours of $\psi' + \psi'^b - cy$ for

$$k/k_c = 0.25, \quad u'_*/\nu' k_c = 8, 12, \quad ka = 0.1;$$
$$k/k_c = 1, \quad u'_*/\nu' k_c = 15, 25, \quad ka = 0.2$$

in the coordinates moving with the phase velocity of the surface waves. In all cases there is a circulation of air at the height where the wind speed in the fixed coordinates equals the phase velocity. This height decreases as the wind speed increases.

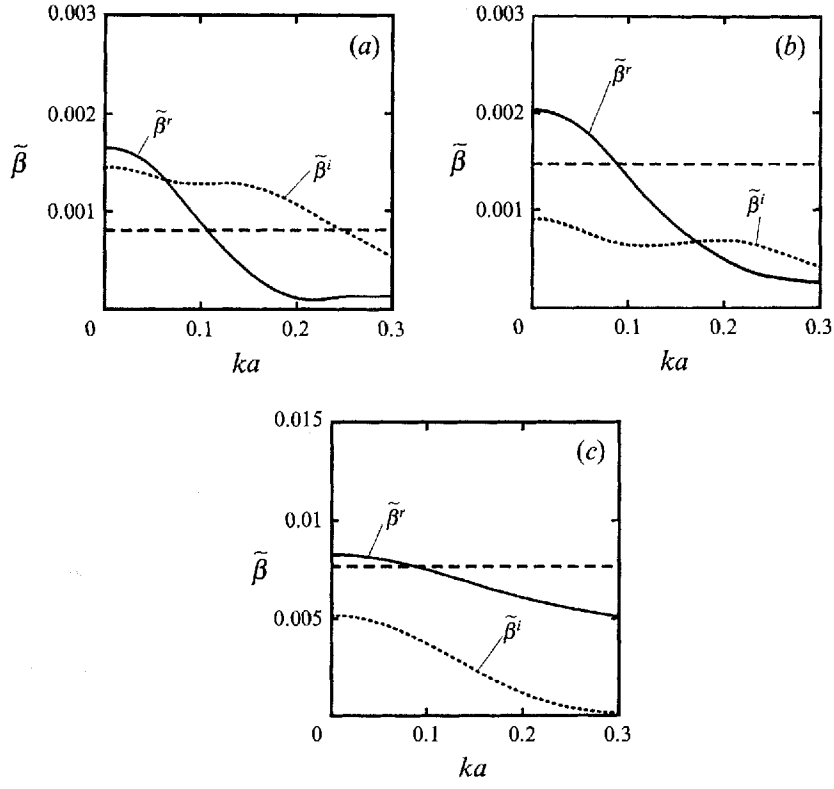

FIGURE 2. Nonlinear energy input rate $\tilde{\beta}^r$ (——), imaginary part of wind forcing $\tilde{\beta}^i$ (----), and dissipation rate (—), as functions of wave slope ka. (*a*) $k/k_c = 0.2$, $u'_*/\nu' k_c = 10$; (*b*) $k/k_c = 0.3$, $u'_*/\nu' k_c = 10$; (*c*) $k/k_c = 0.9$, $u'_*/\nu' k_c = 22$.

3.4. *Effective sea roughness*

Recall from (3.8*a*) that the wave perturbed horizontal velocity $\partial\psi'/\partial\eta$ is finite at $\eta = \infty$. This corresponds to a finite wind velocity shift caused by waves. In the theory of fully turbulent shear flow over a rough bed, the dimensional velocity U' at any dimensional height Y is known to be

$$\frac{U'_{\text{rough}}}{u'_*} = \frac{1}{\kappa}\ln\frac{Y}{k_s} + 8.5 \tag{3.18}$$

(Schlichting 1955), where k_s is the equivalent surface roughness. For a fixed u'_*, the velocity decreases as the roughness k_s increases. On the other hand, the velocity profile over a smooth surface is

$$\frac{U'_{\text{smooth}}}{u'_*} = \frac{1}{\kappa}\ln\frac{u'_* Y}{\nu'} + 5.5 \tag{3.19}$$

(Schlichting 1955). Equating their difference, which is due to the roughness, to the velocity shift due to waves,

$$u'_{\text{rough}} - u'_{\text{smooth}} = \frac{u'_*}{(g/k)^{\frac{1}{2}}}\left[3.0 - \frac{1}{\kappa}\ln\frac{u'_* k_s}{\nu'}\right] = \left(\frac{\partial\psi'}{\partial\eta}\right)_{\eta=\infty}, \tag{3.20}$$

we can calculate the equivalent roughness k_s of a wavy surface to wind, for given wavelength, wave amplitude, and wind shear. Figure 4 shows the normalized

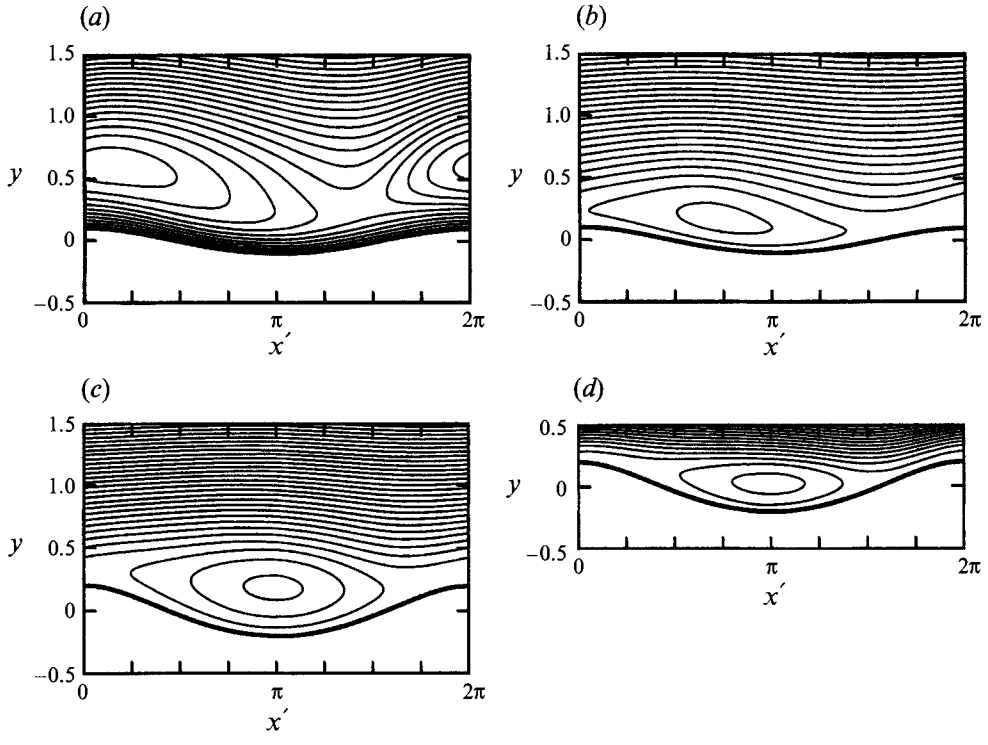

FIGURE 3. Stream-function contours of air flow over surface waves. Vertical scale is stretched by a factor of 2. (*a*) $k/k_c = 0.25$, $u'_*/\nu' k_c = 8$, $\Delta\psi' = 0.02$, $ka = 0.1$; (*b*) $k/k_c = 0.25$; $u'_*/\nu' k_c = 12$, $\Delta\psi' = 0.06$, $ka = 0.1$; (*c*) $k/k_c = 1$, $u'_*/\nu' k_c = 15$, $\Delta\psi' = 0.12$, $ka = 0.2$; (*d*) $k/k_c = 1$, $u'_*/\nu' k_c = 25$, $\Delta\psi' = 0.12$, $ka = 0.2$.

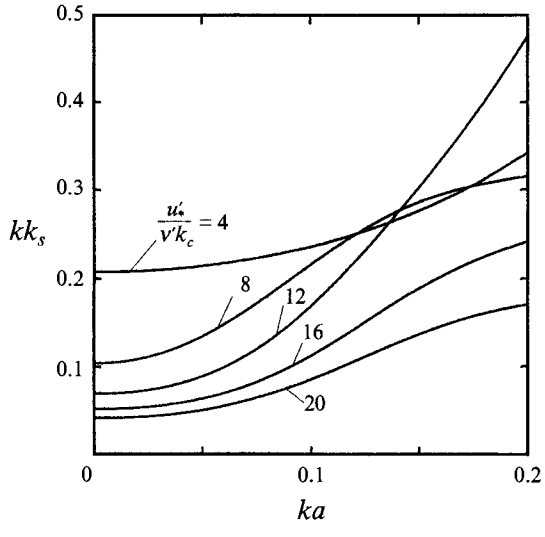

FIGURE 4. Normalized equivalent roughness kk_s as a function of wave slope ka for different values of normalized friction velocity $u'_*/\nu' k_c$; $k/k_c = 0.25$.

roughness kk_s against wave slope ka for $k/k_c = 0.25$. The roughness length increases rapidly with the wave amplitude at around $u'_*/\nu' k_c = 12$. For stronger or weaker wind the effect of waves is less significant. For very short gravity–capillary waves ($k/k_c > 1$), the roughness is relatively insensitive to the wave amplitude and is not presented here.

4. Wave motion in water

Let us define the stream function ψ^b for the basic drift current in the absence of waves, and ψ for the wave-induced flow, by

$$u^b = \epsilon \frac{\partial \psi^b}{\partial y}, \quad u = \epsilon \frac{\partial \psi}{\partial y}, \quad v = -\epsilon \frac{\partial \psi}{\partial x}, \tag{4.1}$$

and rescale the surface displacement by

$$\zeta = \epsilon \tilde{\xi} \tag{4.2}$$

so that $\tilde{\xi} = O(1)$. Away from the viscous surface boundary layer, the outer solution, denoted by ψ_o, is governed by the following vorticity equation:

$$\nabla^2 \frac{\partial \psi_o}{\partial t} - \epsilon \frac{\partial(\psi_o, \nabla^2 \psi^b)}{\partial(x,y)} - \epsilon \frac{\partial(\psi^b, \nabla^2 \psi_o)}{\partial(x,y)} - \epsilon \frac{\partial(\psi_o, \nabla^2 \psi_o)}{\partial(x,y)} = N\epsilon^3 \nabla^2 \nabla^2 \psi_o. \tag{4.3}$$

It can be shown (see Hara & Mei 1991) that the viscous boundary-layer correction leads to an apparent displacement of the free surface, and the kinematic boundary condition on the free surface becomes

$$\frac{\partial \tilde{\xi}}{\partial t} + \epsilon \frac{\partial(\psi_o + \psi^b)}{\partial y} \frac{\partial \tilde{\xi}}{\partial x} + \frac{\partial \psi_o}{\partial x} = -\epsilon^3 NA\, \mathrm{e}^{\mathrm{i}(x-ct)} + * + O(\epsilon^4, \epsilon^3 \delta'), \quad y = \epsilon \tilde{\xi}. \tag{4.4}$$

On the other hand the normal-stress boundary condition is not affected by the boundary-layer correction, and yields

$$\begin{aligned} &\frac{\partial^2 \psi_o}{\partial y\, \partial t} + \epsilon \frac{\partial(\psi_o + \psi^b)}{\partial y} \frac{\partial^2 \psi_o}{\partial y\, \partial x} - \epsilon \frac{\partial \psi_o}{\partial x} \frac{\partial^2 (\psi_o + \psi^b)}{\partial y^2} - N\epsilon^3 \nabla^2 \frac{\partial \psi_o}{\partial y} \\ &\quad + \epsilon \left(-\frac{\partial^2 \psi_o}{\partial x\, \partial t} - \epsilon \frac{\partial(\psi_o + \psi^b)}{\partial y} \frac{\partial^2 \psi_o}{\partial x^2} + \epsilon \frac{\partial \psi_o}{\partial x} \frac{\partial^2 \psi_o}{\partial x\, \partial y} \right) \frac{\partial \tilde{\xi}}{\partial x} \\ &\quad + \frac{\partial \tilde{\xi}}{\partial x} - 2N\epsilon^3 \frac{\partial^3 \psi_o}{\partial x^2\, \partial y} - \gamma \frac{\partial}{\partial x} \left\{ \frac{\partial^2 \tilde{\xi}}{\partial x^2} \left[1 + \epsilon^2 \left(\frac{\partial \tilde{\xi}}{\partial x} \right)^2 \right]^{-\frac{3}{2}} \right\} \\ &= N\epsilon^3 \sum_{n=-\infty}^{\infty} p_n\, \mathrm{e}^{\mathrm{i}n(x-ct)} + O(\epsilon^4), \quad y = \epsilon \tilde{\xi}. \end{aligned} \tag{4.5}$$

At infinity the wave motion decays to zero;

$$\psi_o = 0, \quad y = -\infty. \tag{4.6}$$

We now solve the outer solution by perturbations. Since the lengthy procedure is similar to that for pure gravity waves (Hara & Mei 1991), only the final results are

presented. We mention in particular that at $O(\epsilon)$, quadratic nonlinearity on the free surface introduces an apparent mean tangential stress contributed by wind/wave and wave/wave interaction. This leads to a slowly varying current diffusing vorticity downward.

Finally, one gets from solvability conditions a pair of evolution equations for A and the stream function for a wave-induced inviscid current $\bar{\psi}_{20}$, valid for $\epsilon^3 t = O(1)$. The first envelope equation is

$$\begin{aligned}
&\frac{\partial A}{\partial t_1}+\left[\frac{1+3\gamma}{2(\gamma+1)^{\frac{1}{2}}}+\epsilon\kappa_{10}+\epsilon^2(\kappa_{11}+\kappa_{50})\right]\frac{\partial A}{\partial x_1}\\
&\quad+\mathrm{i}[\kappa_{00}+\epsilon(\kappa_{01}+\kappa_{20})+\epsilon^2(\kappa_{02}+\kappa_{21}+\kappa_{40})]\,A\\
&\quad+\mathrm{i}(\epsilon\alpha_0+\epsilon^2\kappa_{30})\frac{\partial^2 A}{\partial x_1^2}+\mathrm{i}(\epsilon\alpha_1+\epsilon^2\kappa_{60})\,|A|^2 A\\
&\quad+\epsilon^2\beta_0\frac{\partial^3 A}{\partial x_1^3}+\epsilon^2\beta_1|A|^2\frac{\partial A}{\partial x_1}+\epsilon^2\beta_2 A^2\frac{\partial A^*}{\partial x_1}+\epsilon^2\mathrm{i}\left(\frac{\partial\bar{\psi}_{20}}{\partial y_1}\right)_{y_1=0}A\\
&\quad-\epsilon^2 N(\beta^r-2+\mathrm{i}\beta^i)\,A=0,
\end{aligned}\tag{4.7}$$

and the second evolution equation is for the wave-induced current $\bar{\psi}_{20}(x_1, y_1, t_1)$:

$$\frac{\partial^2\bar{\psi}_{20}}{\partial x_1^2}+\frac{\partial^2\bar{\psi}_{20}}{\partial y_1^2}=0,\tag{4.8}$$

with boundary conditions

$$\frac{\partial\bar{\psi}_{20}}{\partial x_1}=-\frac{c}{2}\frac{\partial|A|^2}{\partial x_1},\quad y_1=0\tag{4.9}$$

and

$$\bar{\psi}_{20}=0,\quad y_1=-\infty,\tag{4.10}$$

where $x_1=\epsilon x$, $y_1=\epsilon y$, and $t_1=\epsilon t$. All the coefficients in (4.7) are listed in the Appendix. The coefficients α_0, α_1, β_0, β_1, and β_2 are functions of the surface tension parameter γ alone. All the κ are the consequences of the mean water current. More specifically $\kappa_{00}, \kappa_{10}, \ldots, \kappa_{60}$ are due to the basic wind-induced current ψ^b without the waves, and $\kappa_{01}, \kappa_{11}, \kappa_{21}$ are due to the wave-modified current ψ^q whose solution is given in (A 29). The coefficient κ_{02} depends on the higher-order modified current ψ_{30}. The last term in (4.7) represents wind forcing and viscous dissipation, where β^r, β^i are related to $\tilde{\beta}^r$, $\tilde{\beta}^i$ defined in §3 by

$$\beta^r=\frac{1}{2\sigma^2}\tilde{\beta}^r,\quad \beta^i=\frac{1}{2\sigma^2}\tilde{\beta}^i.\tag{4.11}$$

Both β^r and β^i are of $O(1)$ and are real nonlinear functions of the absolute wave amplitude $|A|$ for prescribed wind shear and wavenumber, calculated numerically in §3. The real part β^r and the imaginary part β^i are responsible for the growth and the phase shift of the wave amplitude A respectively.

With reference to (4.7) let us define the modified phase velocity $\tilde{c}$ and group velocity $\tilde{c}_g$ as follows:

$$\tilde{c}\equiv c+\epsilon\tilde{\tilde{c}},\quad \tilde{\tilde{c}}=\kappa_{00}+\epsilon(\kappa_{01}+\kappa_{20})+\epsilon^2(\kappa_{02}+\kappa_{21}+\kappa_{40})+O(\epsilon^3),\tag{4.12}$$

and

$$\tilde{c}_g\equiv\frac{1+3\gamma}{2(\gamma+1)^{\frac{1}{2}}}+\epsilon\kappa_{10}+\epsilon^2(\kappa_{11}+\kappa_{50})+O(\epsilon^3).\tag{4.13}$$

By introducing the transformation

$$A = \tilde{A}(\xi, \tau) \exp\left[-\mathrm{i}\int^{t_1} \tilde{\tilde{c}}\, \mathrm{d}t_1\right] \tag{4.14}$$

with

$$\xi = x_1 - \int^{t_1} \tilde{c}_g\, \mathrm{d}t_1, \quad \tau = \epsilon t_1 \tag{4.15a, b}$$

the evolution equation (4.7) is simplified to

$$\frac{\partial \tilde{A}}{\partial \tau} + \mathrm{i}(\alpha_0 + \epsilon\kappa_{30})\frac{\partial^2 \tilde{A}}{\partial \xi^2} + \mathrm{i}(\alpha_1 + \epsilon\kappa_{60})|\tilde{A}|^2 \tilde{A} + \epsilon\beta_0 \frac{\partial^3 \tilde{A}}{\partial \xi^3} + \epsilon\beta_1 |\tilde{A}|^2 \frac{\partial \tilde{A}}{\partial \xi} + \epsilon\beta_2 \tilde{A}^2 \frac{\partial \tilde{A}^*}{\partial \xi}$$

$$+ \epsilon\mathrm{i}\left(\frac{\partial \bar{\psi}_{20}}{\partial y_1}\right)_{y_1=0} \tilde{A} - \epsilon N(\beta^r - 2 + \mathrm{i}\beta^i)\tilde{A} = 0, \tag{4.16}$$

where κ_{30}, κ_{60} are functions of the basic current ψ^b. The equations for $\bar{\psi}_{20}$ are unchanged except that x_1 is substituted by ξ.

If the effects of wind and viscosity are neglected ($N = \beta^r = \beta^i = \kappa_{30} = \kappa_{60} = 0$), these equations reduce to those by Hogan (1985). If surface tension vanishes ($\gamma = 0$) the results in Hara & Mei (1991) for gravity waves are recovered. Note that in (4.16) only the fourth, fifth, and sixth terms may yield the asymmetric evolution of a wave spectrum over the timescale of $\epsilon\tau = O(1)$.

Before solving the evolution equations the coefficients κ_{30} and κ_{60} must be calculated. Referring to the Appendix, first the functions g_{00} and g_{10} are solved by finite differences from (A 22), (A 24), and (A 27) with $u^b = \epsilon\, \partial\psi^b/\partial y$ given in §2. The results are then introduced in (A 13), (A 16), (A 17), (A 20) to calculate κ_{30} and κ_{60}. In the range of parameters examined, κ_{30} is always negative and κ_{60} is mostly positive, except for the case of the longest wave ($k/k_c = 0.2$) and very strong wind ($u'_*/\nu' k_c = 15$) where κ_{60} is also negative.

The coefficients $\kappa_{00}, \kappa_{20}, \kappa_{40}$ in the phase velocity $\tilde{c}$ and κ_{10}, κ_{50} in the group velocity $\tilde{c}_g$ are also calculated from ψ^b. The calculation of κ_{01}, κ_{11}, and κ_{21} depends on ψ^q given in (A 29) which depends on the solution to the evolution equation (4.16) through the modified shear $q_0(\tau)$. The calculation of the phase velocity $\tilde{c}$ at $O(\epsilon^3)$ requires knowledge of κ_{02} which depends on the higher-order analysis in air. This will not be pursued in this study, since the evolution of the absolute wave amplitude $|A|$ can be solved without knowledge of the modified phase velocity (cf. (4.14)).

5. Initial instability of sideband disturbances

Based on the evolution equations (4.8)–(4.10) (with x_1 replaced by ξ) and (4.16), we now examine the initial growth of the Benjamin–Feir instability. First we solve for the spatially uniform Stokes wave train A_0 by setting $\partial/\partial\xi = \bar{\psi}_{20} = 0$ in (4.16). The solution may be written as

$$A_0 = B \exp\left\{\mathrm{i}\int^{\tau} [(\alpha_1 + \epsilon\kappa_{60})B^2 - \epsilon N\beta^i(B)]\, \mathrm{d}\tau\right\}, \tag{5.1}$$

where the amplitude B satisfies

$$\partial B/\partial\tau - \epsilon N[\beta^r(B) - 2]B = 0. \tag{5.2}$$

In general B grows or decays slowly over the timescale of $\epsilon\tau = t_3 = O(1)$ from its initial value which is set to be unity, i.e. ϵ is set to be the initial wave steepness.

To study the initial growth rate of instability, we let

$$\tilde{A} = A_0(1+A'), \quad \bar{\psi}_{20} = \bar{\psi}'_{20}, \tag{5.3}$$

where A' and $\bar{\psi}'_{20}$ are small perturbations. Let A' be further separated into real and imaginary parts

$$A' = A'_r + \mathrm{i}A'_i, \tag{5.4}$$

both of which are assumed to be of the form

$$A'_r = \mathrm{Re}\, a'_r \mathrm{e}^{\mathrm{i}(K\xi - \Omega\tau)}, \quad A'_i = \mathrm{Re}\, a'_i \mathrm{e}^{\mathrm{i}(K\xi-\Omega\tau)}, \tag{5.5}$$

where $K > 0$ is the wavenumber of the disturbances, and Ω is the complex frequency. Then Ω is solved to be

$$\Omega = \frac{1}{2}\left[-2\epsilon\beta_0 K^3 + 2\epsilon\beta_1 K + \mathrm{i}\epsilon N\left(\frac{\mathrm{d}\beta^r}{\mathrm{d}B}\right)_{B=1}\right]$$
$$\pm\left[(\alpha_0 + 2\epsilon\kappa_{30})\alpha_0 K^4 - 2(\alpha_0\alpha_1 + \epsilon\alpha_0\kappa_{60} + \epsilon\alpha_1\kappa_{30})K^2 + \epsilon c\alpha_0 K^3 + \epsilon N\alpha_0\left(\frac{\mathrm{d}\beta^i}{\mathrm{d}B}\right)_{B=1}K^2\right]^{\frac{1}{2}} \tag{5.6}$$

to the accuracy of $O(\epsilon)$. If wind and viscous dissipation are neglected ($N = \beta^r = \beta^i = \kappa_{30} = \kappa_{60} = 0$) in (5.6), Hogan's result is recovered,

$$\Omega = -\epsilon\beta_0 K^3 + \epsilon\beta_1 K \pm (\alpha_0^2 K^4 - 2\alpha_0\alpha_1 K^2 + \epsilon c\alpha_0 K^3)^{\frac{1}{2}}. \tag{5.7}$$

If we further set $\epsilon = 0$, the nonlinear evolution equation reduces to the cubic Schrödinger equation (Djordjevic & Redekopp 1977) and

$$\Omega = \pm(\alpha_0^2 K^4 - 2\alpha_0\alpha_1 K^2)^{\frac{1}{2}} = \pm[\alpha_0^2 K^2(K^2 - 2\alpha_1/\alpha_0)]^{\frac{1}{2}}. \tag{5.8}$$

For instability $\mathrm{Im}(\Omega) > 0$. For $\alpha_1/\alpha_0 \leqslant 0$, the sidebands are stable according to the cubic Schrödinger equation. Referring to (A 1) and (A 2) for the coefficients α_0 and α_1, this criterion is satisfied when $0.155 < \gamma = (k/k_c)^2 < 0.5$. In particular α_1 becomes unbounded at $\gamma = 0.5$. Hence

$$\begin{aligned} k/k_c &< 0.393 && : \text{instability},\\ 0.393 < k/k_c &< 0.707 && : \text{stability},\\ 0.707 < k/k_c &&& : \text{instability}. \end{aligned}$$

Note first that $k/k_c = 0.707$ corresponds to Wilton's ripple. In this case waves with wavenumbers k and $2k$ are resonantly coupled over the timescale of $t_1 = \epsilon t$; the nonlinear Schrödinger equation breaks down. Janssen (1986) has shown that wind can trigger this subharmonic resonance (energy transfer from $k/k_c = 1.414$ to $k/k_c = 0.707$), leading to period doubling. This case is excluded here.

With the $O(\epsilon)$ terms which include the wind effect, the threshold $k/k_c = 0.393$ is modified by $O(\epsilon)$, while the coefficient α_1 remains unbounded at $k/k_c = 0.707$. Therefore there is no sideband instability for $0.393 + O(\epsilon) < k/k_c < 0.707$, and we only consider the unstable ranges from here on.

Without wind and damping it has been shown by Hogan (1985) from (5.7) that the maximum sideband growth rate is reduced as ϵ increases for relatively long waves

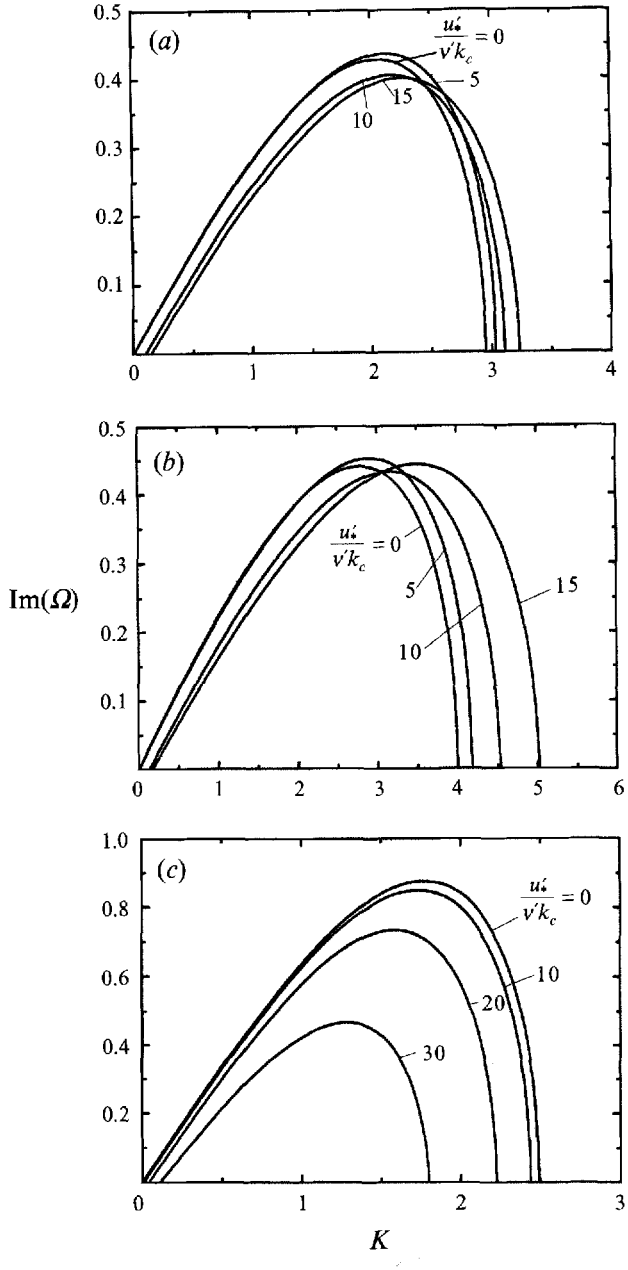

FIGURE 5. Instability growth rate $\mathrm{Im}(\Omega)$ as a function of wavenumber K for various normalized friction velocities $u'_*/v'k_c$; $\epsilon = 0.1$: (*a*) $k/k_c = 0.2$, (*b*) $k/k_c = 0.3$, (*c*) $k/k_c = 0.9$.

($k/k_c < 0.393 + O(\epsilon)$), but is increased for short waves ($k/k_c > 0.707$). We have found that the same trends remain at all the wind speeds which are within the range of our theoretical assumption.

On the other hand at a given initial wave slope the influence of wind on the initial growth rate of the unstable mode is not trivial. We plot in figure 5 the growth rate $\mathrm{Im}(\Omega)$ as a function of unstable wavenumber K for various wind stresses and for a fixed wave slope $\epsilon = 0.1$. For rather long waves $k/k_c = 0.2$ and 0.3, the wavenumber K of the

least-stable mode increases as the wind stress increases. However, no systematic trends are observed for the growth rate Im (Ω) of the least-stable mode. For short waves with $k/k_c = 0.9$, instability is strongly suppressed by wind.

6. Nonlinear stage of Benjamin–Feir instability

We now examine the nonlinear stage of sideband instability on the timescale of $t = O(1/\epsilon^3)$, by numerically integrating the coupled equations for the wave amplitude $\tilde{A}$ and the wave-induced current $\bar{\psi}_{20}$. First the least-stable wavenumber K of the instability is calculated from the result in §5 for given relative wavenumber k/k_c, normalized friction velocity $u'_*/\nu' k_c$, and initial wave slope ϵ of a uniform wave train. The initial condition for $\tilde{A}$ is then specified so that the maximum of the disturbance $|A'|$ is 0.1. We note that if the amplitude of the initial disturbance is reduced, the initial growth is delayed but the subsequent evolution remains similar. The pseudo-spectral method employed before by Lo & Mei (1985) is used, where $\tilde{A}$ is expanded in a Fourier series with coefficients B_ν, $\nu = 0, \pm 1, \pm 2, \ldots$. For further details see Hara (1990) or Hara & Mei (1991).

As a reference we first display in figure 6(*a–c*) the nonlinear evolution without wind or damping for $\epsilon = 0.1$. Recurrence is always present as in the case of gravity waves (Lo & Mei 1985). Near the time of maximum modulation, frequency downshift is apparent for long waves with $k/k_c = 0.2$ and 0.3 but there is upshift for the short wave with $k/k_c = 0.9$. The upshift also occurred at $k/k_c = 1.0$ but a slight downshift was observed for very short waves with $k/k_c = 1.75$ (Hara 1990). In all cases the downshift or upshift phenomenon is only a transient phase of a cyclic process.

We now examine the effect of wind and viscous damping. For each of these wavelengths, different wind intensities and wave steepnesses are studied.

(i) $k/k_c = 0.3$, $u'_*/\nu' k_c = 10$

This is a typical case of long waves and weak wind. From figure 2(*b*) the net growth rate becomes zero at $(ka)_{eq} = 0.088$. Let us examine two initial wave slopes (ϵ). With the help of table 1, N is calculated from (2.16).

(*a*) $\epsilon = 0.1$ ($N = 0.37$) (figure 7)

By definition $|\tilde{A}|_{eq} = B_{eq} = (ka)_{eq}/\epsilon = 0.88$. The time evolution of the zeroth, $\pm$first, $\pm$second harmonics ($|B_0|, |B_{\pm 1}|, |B_{\pm 2}|$) are plotted in figure 7(*a*, *b*). At the beginning near-recurrence is observed with the $-$first harmonic (lower sideband) larger than the $+$first (upper sideband). As the evolution proceeds the magnitude of the $-$first harmonic $|B_{-1}|$ continues to grow while all other harmonics die out. At $\tau = 80$ the envelope becomes almost uniform, being dominated by B_{-1}. This is clear evidence of persistent frequency downshift. Towards the end of the computation time the magnitude of B_{-1} approaches $B_{eq} = 0.88$. In figure 7(*c*) the amplitude spectrum of the harmonics ($|B_\nu|, \nu = -10$–10) is plotted at $\tau = 80$, and compared to the initial spectrum indicated by crosses. After downshifting the spectrum remains narrow, indicating the uniform validity of the narrow-band assumption.

(*b*) $\epsilon = 0.045$ ($N = 4.0$) (figure 8)

In this case the initial wave amplitude is reduced. By definition $B_{eq} = (ka)_{eq}/\epsilon$ is now 1.97; i.e. the amplitude of the uniform train would become 1.97 times as large as the original without sideband disturbances. Though the initial steepness is smaller, the ultimate steepness is comparable with the preceding case. From figure 5(*b*),

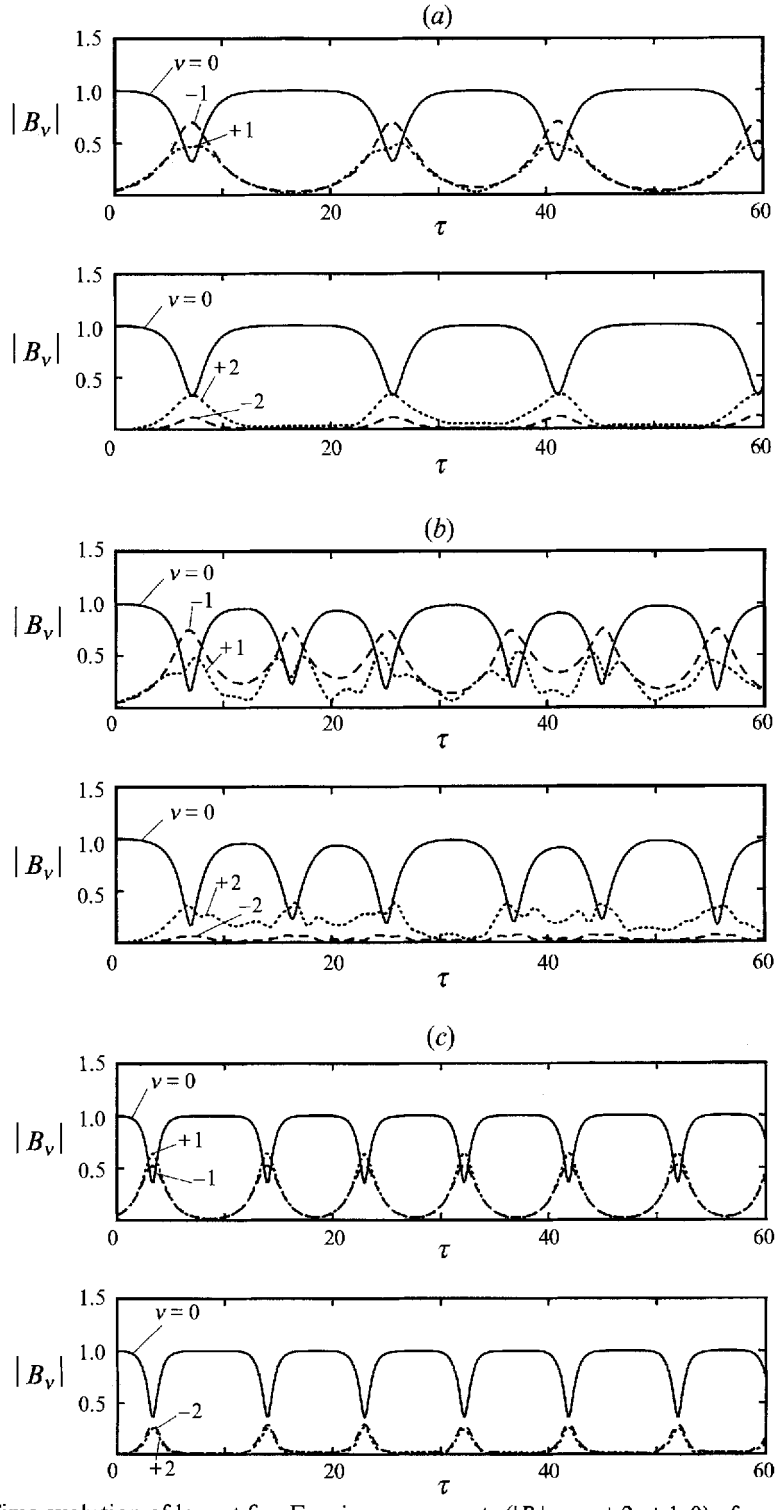

FIGURE 6. Time evolution of lowest five Fourier components ($|B_\nu|$, $\nu = \pm 2, \pm 1, 0$) of wave amplitude $\tilde{A}$ without wind or dissipation; $\epsilon = 0.1$: (*a*) $k/k_c = 0.2$, $K = 2.05$; (*b*) $k/k_c = 0.3$, $K = 2.77$; (*c*) $k/k_c = 0.9$, $K = 1.78$.

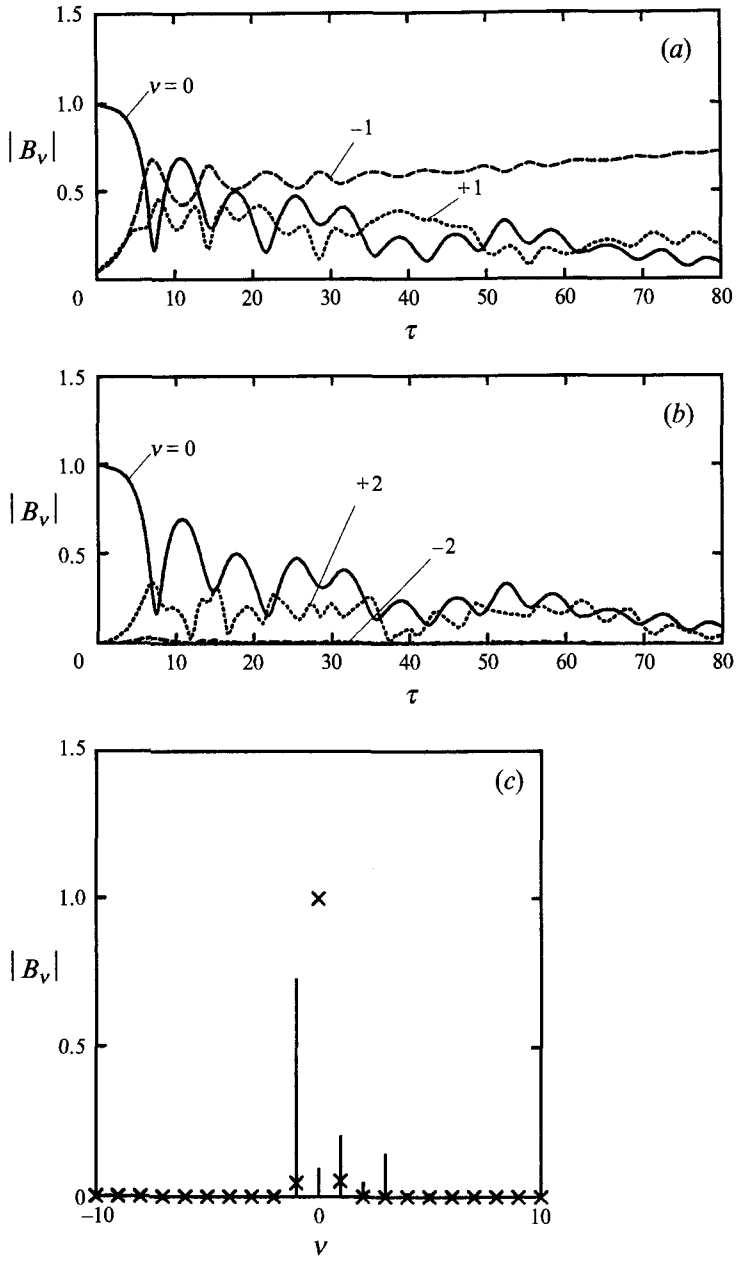

FIGURE 7. (*a*, *b*) Time evolution of lowest five Fourier components ($|B_\nu|$, $\nu = \pm 2, \pm 1, 0$) of wave amplitude $\tilde{A}$. (*c*) Amplitude spectrum of wave amplitude $\tilde{A}$ at $\tau = 80$. $k/k_c = 0.3$, $u'_*/\nu' k_c = 10$, $\epsilon = 0.1$, $K = 3.14$.

wavenumbers up to 1.3–1.4 times that of the least-stable mode are also unstable at $\tau = 0$. Therefore for large τ the maximum unstable wavenumber would be roughly 2.6–2.8 times the initial least-stable wavenumber. In our calculation Fourier components with wavenumbers twice that of the initial disturbances ($B_{\pm 2}$) are therefore expected to become unstable for large τ.

In the initial stage ($\tau \leqslant 15$) the −first harmonic B_{-1} is dominant as in the former case. As the evolution proceeds, the −second harmonic B_{-2} also begins to grow

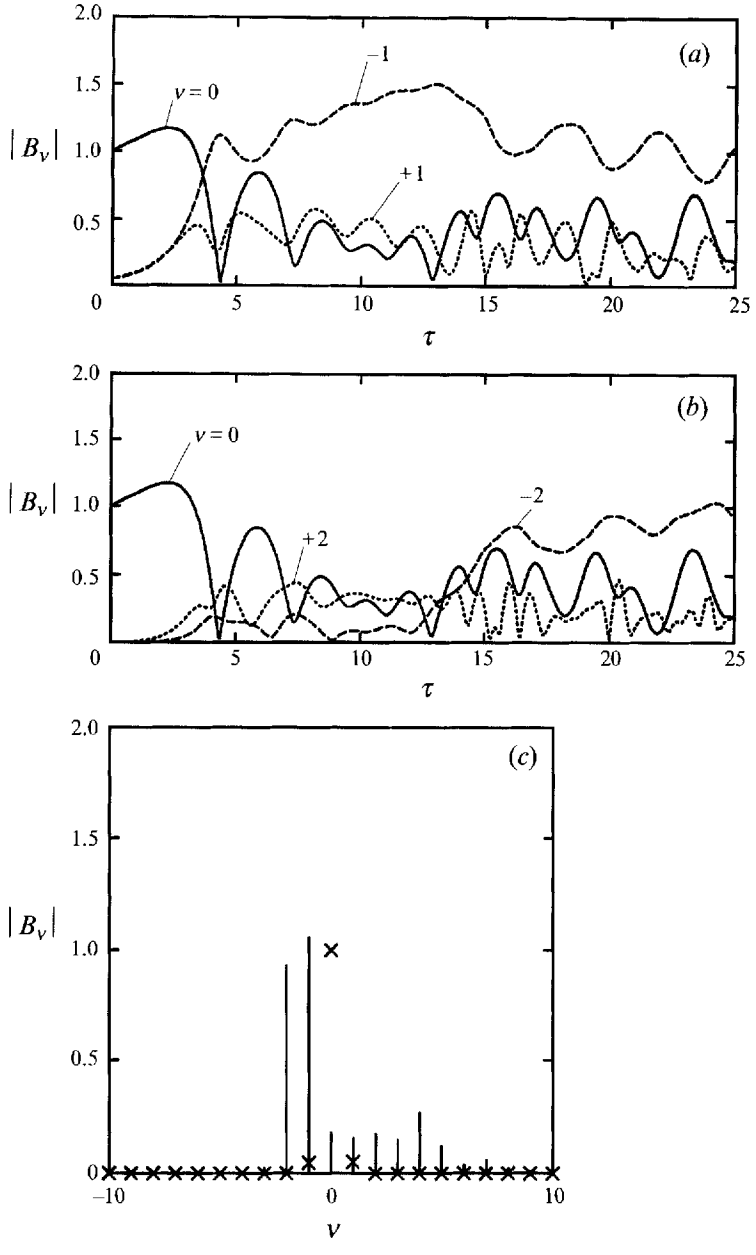

FIGURE 8. As figure 7 but at $\tau = 25$. $k/k_c = 0.3$, $u'_*/\nu' k_c = 10$, $\epsilon = 0.045$, $K = 3.68$.

steadily. The plot of the final amplitude spectrum figure 8(*c*) suggests that the peak frequency is now shifting to $\nu = -2$ from $\nu = -1$, with the rest of the harmonics being relatively small.

(ii) $k/k_c = 0.3, u'_*/\nu' k_c = 12$

With the same wavenumber we now examine a stronger wind. The equilibrium wave steepness is calculated to be $(ka)_{eq} = 0.132$. Let us now consider two initial steepnesses.

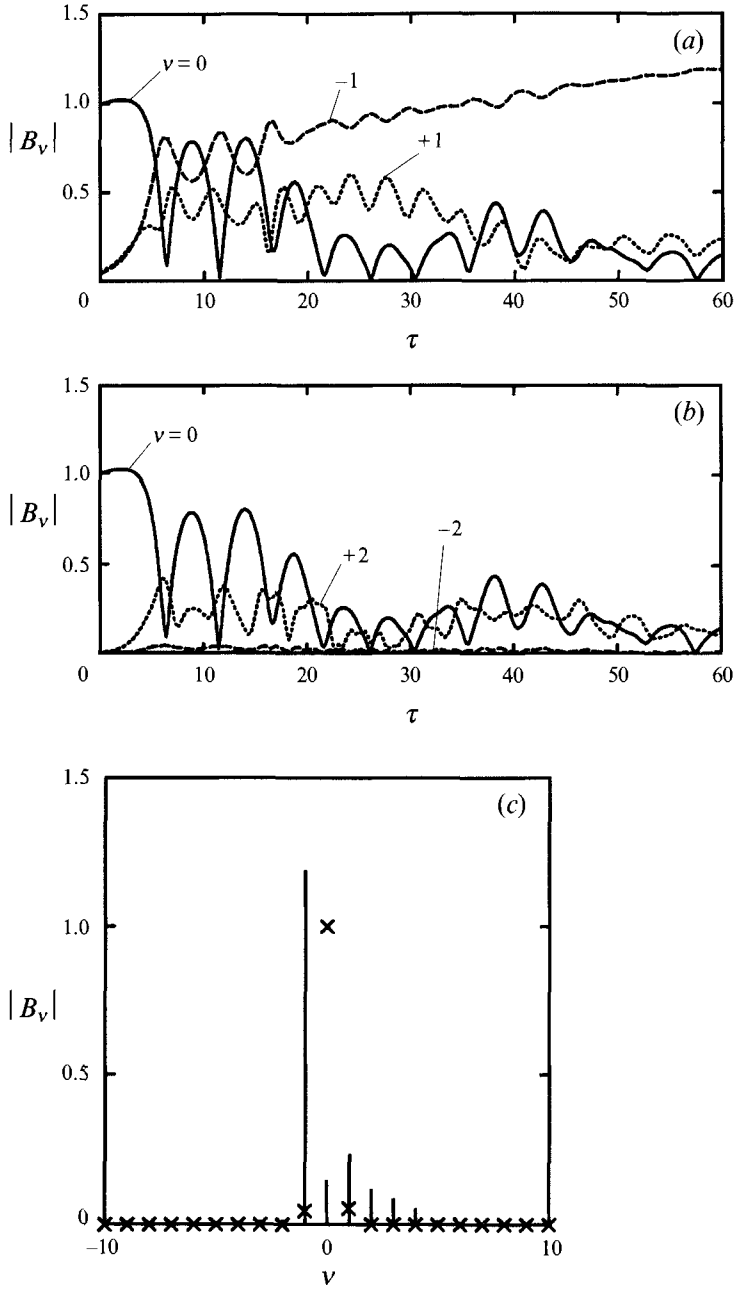

FIGURE 9. As figure 7 but at $\tau = 60$. $k/k_c = 0.3$, $u'_*/\nu' k_c = 12$, $\epsilon = 0.1$, $K = 3.27$.

(*a*) $\epsilon = 0.1$ ($N = 0.37$) (figure 9)

For this small increase in wind strength, the frequency downshift becomes even stronger than the case (1.1) which has the same initial wave slope. For large τ the $-$first harmonic B_{-1} becomes dominant and approaches the equilibrium amplitude $B_{eq} = 1.32$.

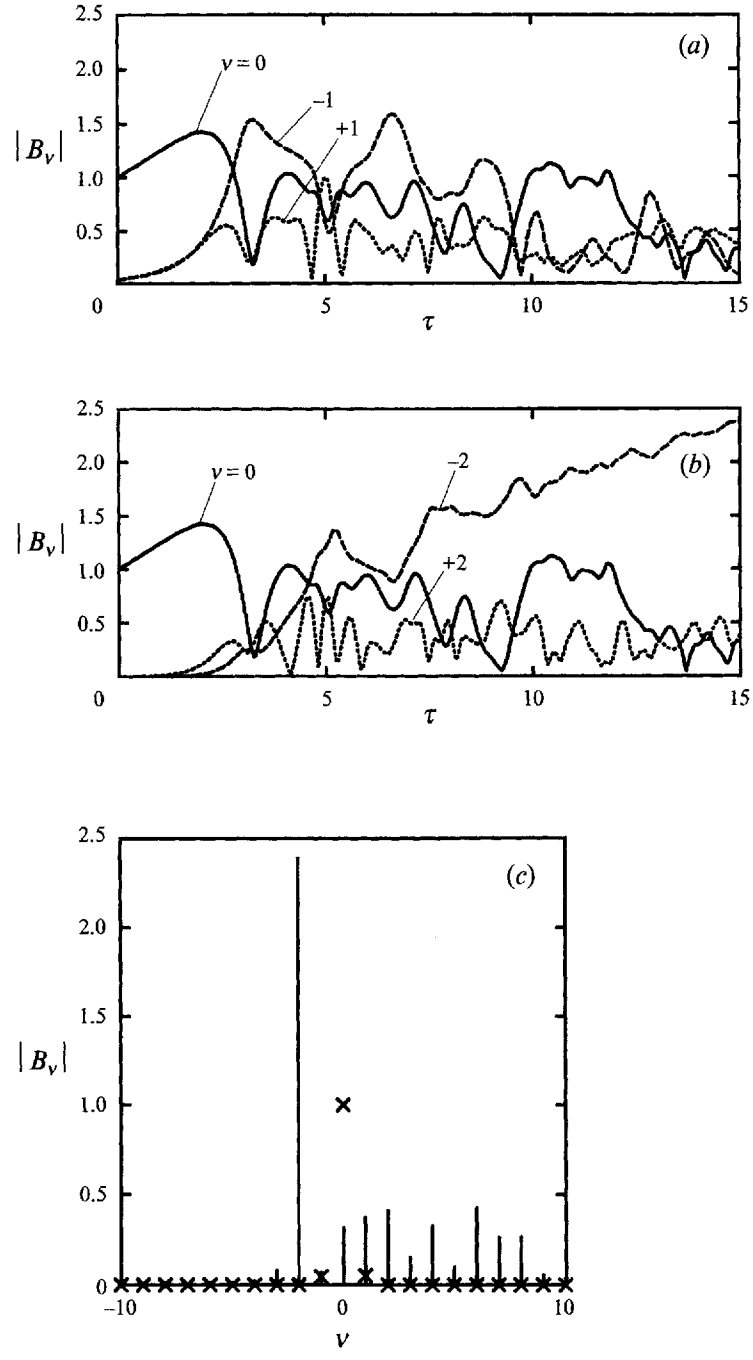

FIGURE 10. As figure 7 but at $\tau = 15$. $k/k_c = 0.3$, $u'_*/\nu' k_c = 12$, $\epsilon = 0.045$, $K = 3.85$.

(*b*) $\epsilon = 0.045$ ($N = 4.0$) (figure 10)

For this case of smaller initial wave slope, the $-$second harmonic quickly takes over the initially dominant $-$first harmonic. The amplitude spectrum at $\tau = 15$ clearly shows that the $-$second harmonic is the peak frequency.

(iii) $k/k_c = 0.2$, $u'_*/\nu' k_c = 10$

We now examine a longer wave with two initial slopes for the weakest wind. The equilibrium wave slope is $(ka)_{eq} = 0.107$ (cf. figure 2*a*).

(*a*) $\epsilon = 0.1$ ($N = 0.20$) (figure 11)

Qualitative features are similar to the case (i)(*a*) for shorter waves. Frequency downshift is evident.

(*b*) $\epsilon = 0.045$ ($N = 2.2$) (figure 12)

As the evolution proceeds, the peak of the spectrum shifts towards the $-$second harmonic. At $\tau = 20$ the amplitude spectrum (figure 12*c*) shows that the $-$third harmonic also has relatively large amplitude, although the spectrum is rather broad.

(iv) $k/k_c = 0.9$, $u'_*/\nu' k_c = 22$ (figure 13)

A much shorter wavelength in the second zone of instability is now examined. Since damping is now large, a much stronger wind is needed to see interesting physics. We present in figure 13 results for $\epsilon = 0.1$ ($N = 1.91$). Throughout the evolution there is a weak frequency upshift, i.e. the upper sideband is slightly larger than the lower sideband. Thus the temporary upshift in the case without wind or viscous dissipation (figure 6*c*) is now rendered permanent. For large time the $\pm$first harmonics slowly take over the fundamental harmonic. With a smaller initial wave slope or stronger wind, the results show more complicated evolution patterns with broader amplitude spectra. However, they no longer yield a clear pattern of permanent frequency upshift or downshift even after a long time. Therefore the permanent frequency upshift occurs only in a very narrow range of wind stress and wave steepness.

We have also investigated the case of $k/k_c = 1.75$ and $u'_*/\nu' k_c = 32$–38. At such a short wavelength the air boundary-layer thickness δ' becomes relatively large (~ 0.14). Consequently the contribution of the tangential stress to the wave growth rate becomes significant (see figure 1), while the growth rate becomes less dependent on the wave steepness because the nonlinearity of the modulated air flow, which is estimated by ϵ/δ', is now smaller. Although the theory can easily be modified to include the tangential stress contribution, the resulting physics is less interesting because of the weak nonlinearity of the air flow. For example at $u'_*/\nu' k_c = 32$ and $\epsilon = 0.173$, the nonlinear evolution remains similar to the case of no wind/dissipation at small τ with temporary downshift near the peak of the modulation. Only at very large τ does the weak frequency downshift become permanent. When the initial wave steepness is decreased, or the wind stress is increased, the nonlinear evolution quickly yields a broader amplitude spectrum, hence violates the assumption of narrow-banded waves. These results are recorded in Hara (1990).

Based on the preceding numerical experiments the effects of wind and viscous damping on the nonlinear evolution of sideband instability of gravity–capillary waves may be summarized as follows.

(i) For relatively long gravity–capillary waves of $k/k_c = 0.2$ and 0.3 in the first zone of instability, the evolution pattern is similar to that of gravity waves. Frequency downshift is evident in all cases examined. With a smaller initial wave amplitude the wave energy may downshift to the higher harmonics of the sideband.

(ii) For a short wavelength $k/k_c = 0.9$ in the second zone of instability, moderate wind and damping may enhance frequency upshift, although the range of permanent upshift is very limited. With a sufficiently short wavelength the permanent frequency

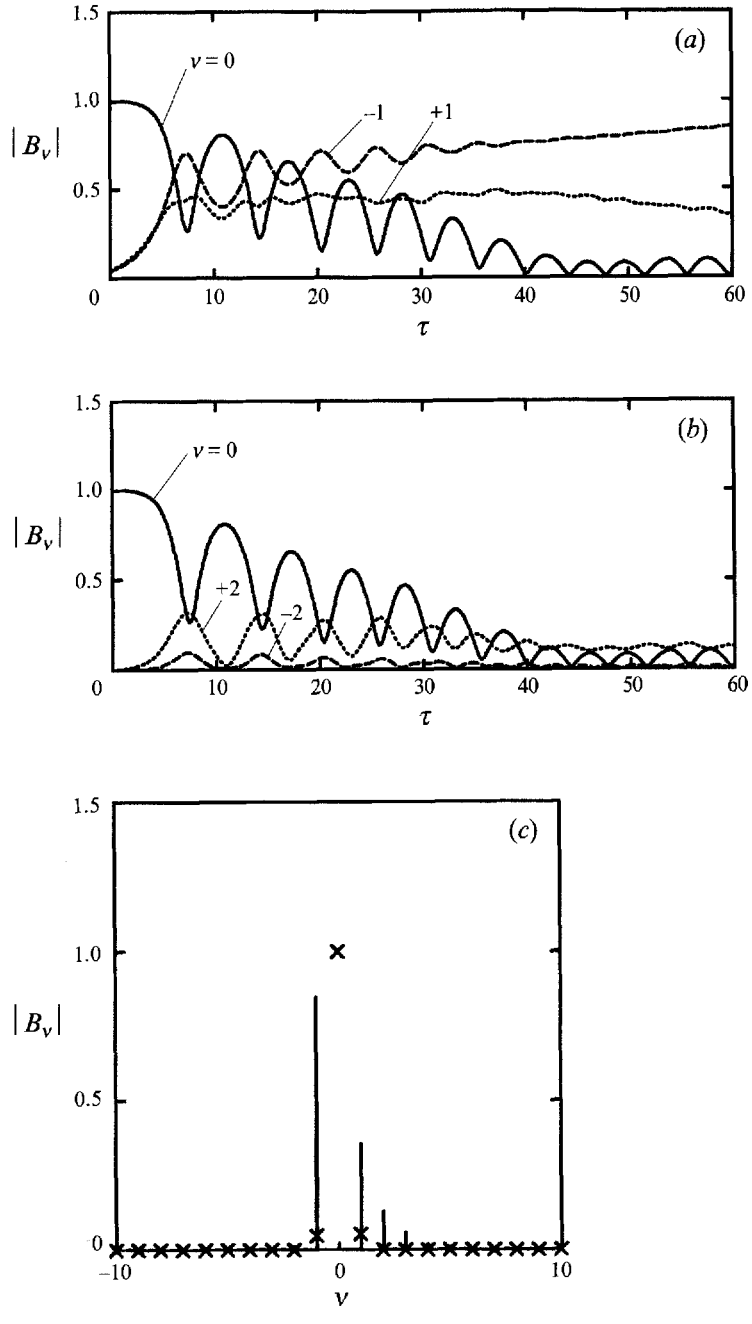

FIGURE 11. As figure 7 but at $\tau = 60$. $k/k_c = 0.2$, $u'_*/\nu' k_c = 10$, $\epsilon = 0.1$, $K = 2.17$.

downshift may prevail again. However, the tendency is very weak because of the weak nonlinearity of the modulated air flow.

(iii) In general as the wind shear increases or the initial wave slope decreases, the evolution becomes more irregular and the amplitude spectrum broadens.

So far our calculations have been performed with a stationary turbulent basic water current. We have also examined a viscous current of an error-function type, which penetrates deeper with time. Although the wind effect on the initial growth rate of

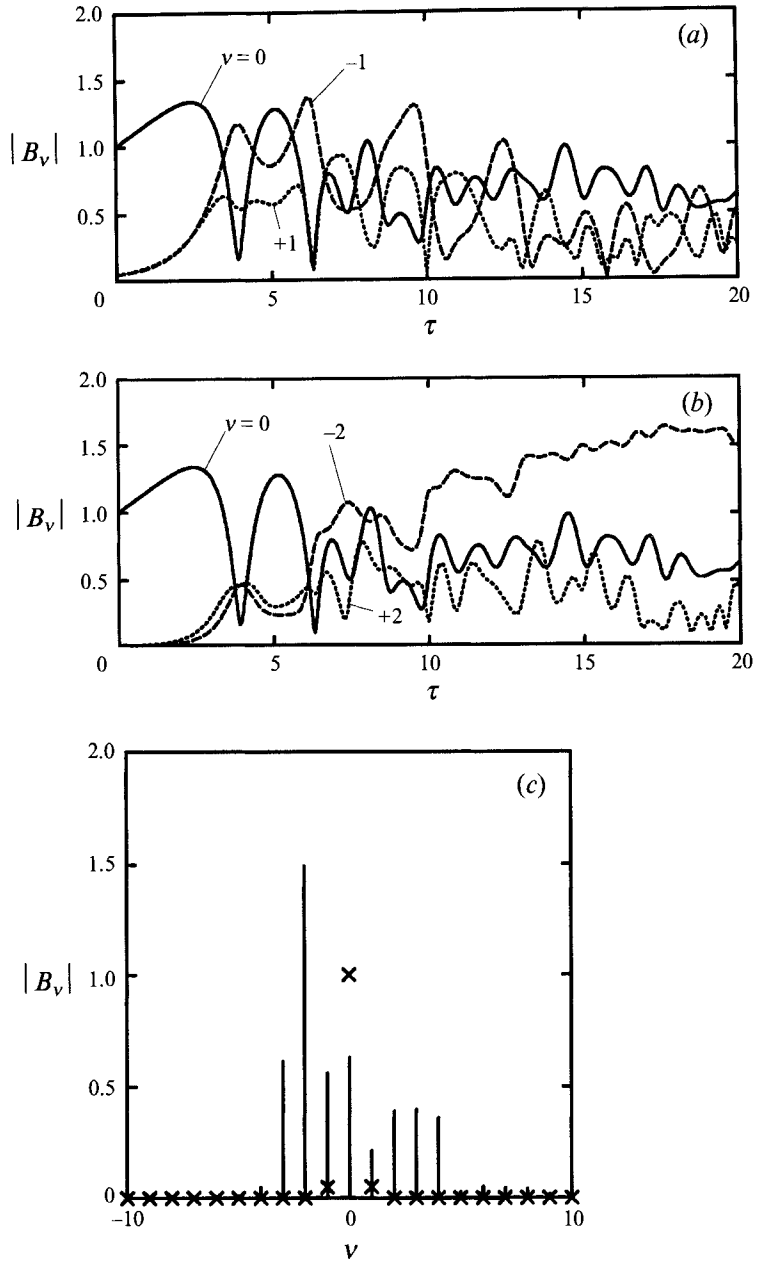

FIGURE 12. As figure 7 but at $\tau = 20$. $k/k_c = 0.2$, $u'_*/\nu' k_c = 10$, $\epsilon = 0.045$, $K = 2.45$.

sideband instability is modified owing to different values of κ_{30} and κ_{60}, the subsequent nonlinear evolution remains similar. Details are given in Hara (1990).

7. Concluding remarks

The wind effect on the evolution of a two-dimensional narrow-banded gravity–capillary wave spectrum has been examined theoretically. The wind strength is assumed to be of such a magnitude that the initial growth of waves occurs on the

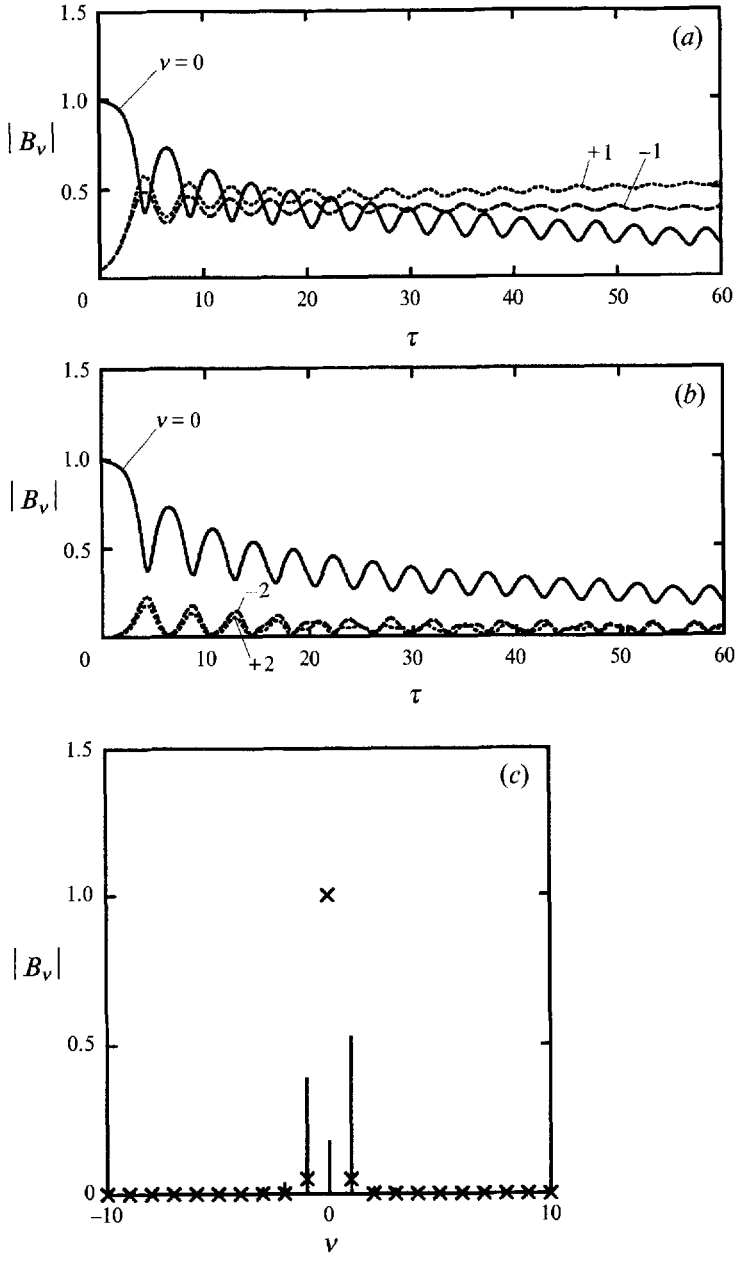

FIGURE 13. As figure 7 but at $\tau = 60$. $k/k_c = 0.9$, $u'_*/\nu' k_c = 22$, $\epsilon = 0.1$, $K = 1.54$.

timescale of the asymmetric evolution of sidebands. The wave growth rate due to wind is found to decrease as the wave steepness increases at a fixed wind stress. This trend is more prominent for longer waves.

By a perturbation analysis up to fourth order in wave steepness, we have modified Hogan's evolution equations for the water wave amplitude $\tilde{A}$ and the wave-induced current $\bar{\psi}_{20}$ valid on the timescale of $t_3 = \epsilon^3 t \leqslant O(1)$. The magnitude of the wind-induced drift is at most comparable with the wave orbital velocity. Wind is found to suppress the initial growth of unstable sidebands for relatively short gravity–capillary

waves ($k/k_c = 0.9$). It yields permanent frequency downshift after a long time for relatively long waves ($k/k_c = 0.2, 0.3$), as in the case for gravity waves, although this tendency is reversed for some short waves within a narrow parameter range. With stronger wind or smaller initial wave steepness the evolution of unstable modes becomes more irregular, and the spectrum of B_ν becomes broader.

Since in nature and in the laboratory, gravity–capillary waves are more likely to be short crested, it appears worthwhile to extend the work of Janssen and the present theory by considering the effect of wind on the evolution of a resonant triad in different directions.

This work has been supported by the Office of Naval Research through the Physical Oceanography Program (Accelerated Research Initiative on Surface Wave Dynamics) during the initial stage, and through the Ocean Engineering Program (Accelerated Research Initiative on Nonlinear Dynamics of Ocean Waves) during the final stage. Partial support has been received from National Science Foundation Programs of Fluids/Particulates/Hydraulic Systems and Ocean Engineering (Grant No. MSME 8813121). Part of the writing was done while T.H. was a post-doctoral scholar at Woods Hole Oceanographic Institution. This is WHOI contribution 7826.

Appendix. Coefficients in the evolution equation

The coefficients α and β are determined by γ only:

$$\alpha_0 = -\frac{3\gamma^2+6\gamma-1}{8(\gamma+1)^{\frac{3}{2}}}, \tag{A 1}$$

$$\alpha_1 = -\frac{2\gamma^2+\gamma+8}{16(\gamma+1)^{\frac{1}{2}}(2\gamma-1)}, \tag{A 2}$$

$$\beta_0 = \frac{(\gamma-1)(\gamma^2+6\gamma+1)}{16(\gamma+1)^{\frac{5}{2}}}, \tag{A 3}$$

$$\beta_1 = -\frac{3(4\gamma^4+4\gamma^3-9\gamma^2+\gamma-8)}{16(\gamma+1)^{\frac{3}{2}}(2\gamma-1)^2}, \tag{A 4}$$

$$\beta_2 = \frac{(\gamma-1)(2\gamma^2+\gamma+8)}{32(\gamma+1)^{\frac{3}{2}}(2\gamma-1)}. \tag{A 5}$$

The coefficients κ are determined by the mean water current:

$$\kappa_{00} = \left(\frac{\partial\psi^b}{\partial y} - \frac{1}{2}\frac{\partial^2\psi^b}{\partial y^2} + \frac{\partial g_{00}}{\partial y}\right)_{y=0}, \tag{A 6}$$

$$\kappa_{01} = \left(\frac{\partial\psi^q}{\partial y} - \frac{1}{2}\frac{\partial^2\psi^q}{\partial y^2} + \frac{\partial g_{01}}{\partial y}\right)_{y=0}, \tag{A 7}$$

$$\kappa_{02} = \left(\frac{\partial\psi_{30}}{\partial y} - \frac{1}{2}\frac{\partial^2\psi_{30}}{\partial y^2}\right)_{y=0} + \int_{-\infty}^{0}\left(\tfrac{1}{2}e^{2y}\frac{\partial^3\psi_{30}}{\partial y^3}\right)dy, \tag{A 8}$$

$$\kappa_{10} = \left(\frac{1}{2}\frac{\partial\psi^b}{\partial y} + \frac{\partial g_{10}}{\partial y}\right)_{y=0}, \tag{A 9}$$

$$\kappa_{11} = \frac{1}{2}\left(\frac{\partial\psi^q}{\partial y}\right)_{y=0} + \int_{-\infty}^{0}\left[-2g_{01} + \left(\frac{\partial\psi^q}{\partial y}\right)_{y=0}e^y + \tfrac{1}{2}y\,e^y\frac{\partial^3\psi^q}{\partial y^3}\right]e^y\,dy, \tag{A 10}$$

$$\kappa_{20} = \left[\frac{1}{8(\gamma+1)^{\frac{1}{2}}}\left(\frac{\partial^2\psi^b}{\partial y^2}+2\frac{\partial g_{00}}{\partial y}\right)^2-\frac{\partial g_{20}}{\partial y}\right]_{y=0}, \tag{A 11}$$

$$\kappa_{21} = \frac{1}{4}\left(\frac{\partial^2\psi^b}{\partial y^2}+2\frac{\partial g_{00}}{\partial y}\right)_{y=0}\left(\frac{\partial^2\psi^q}{\partial y^2}+2\frac{\partial g_{01}}{\partial y}\right)_{y=0}$$
$$+\int_{-\infty}^{0}\left\{g_{01}\frac{\partial^3\psi^b}{\partial y^3}+g_{00}\frac{\partial^3\psi^q}{\partial y^3}+\tfrac{1}{2}e^y\left[\frac{\partial\psi^q}{\partial y}-\left(\frac{\partial\psi^q}{\partial y}\right)_{y=0}\right]\frac{\partial^3\psi^b}{\partial y^3}\right.$$
$$\left.+\tfrac{1}{2}e^y\left[\frac{\partial\psi^b}{\partial y}-\left(\frac{\partial\psi^b}{\partial y}\right)_{y=0}\right]\frac{\partial^3\psi^q}{\partial y^3}\right\}e^y\,dy, \tag{A 12}$$

$$\kappa_{30} = \frac{1}{c}\int_{-\infty}^{0}\tilde{\kappa}_{30}e^y\,dy, \tag{A 13}$$

$$\kappa_{40} = \frac{1}{c}\left[\left(\frac{\partial g_{00}}{\partial y}\frac{\partial g_{20}}{\partial y}+\frac{1}{2}\frac{\partial^2\psi^b}{\partial y^2}\frac{\partial g_{20}}{\partial y}\right)_{y=0}\right.$$
$$\left.+\left(\frac{\partial g_{00}}{\partial y}+\frac{1}{2}\frac{\partial^2\psi^b}{\partial y^2}-\frac{\partial\psi^b}{\partial y}\right)_{y=0}\int_{-\infty}^{0}\tilde{\kappa}_{70}e^y\,dy+\int_{-\infty}^{0}\tilde{\kappa}_{40}e^y\,dy\right], \tag{A 14}$$

$$\kappa_{50} = -\frac{1}{16c^4}\left(\frac{\partial^2\psi^b}{\partial y^2}+2\frac{\partial g_{00}}{\partial y}\right)_{y=0}\left[8c^3\left(\frac{\partial g_{10}}{\partial y}-\frac{1}{2}\frac{\partial\psi^b}{\partial y}\right)\right.$$
$$\left.+c(1+3\gamma)\left(\frac{\partial^2\psi^b}{\partial y^2}+2\frac{\partial g_{00}}{\partial y}\right)\right]_{y=0}-\frac{1+3\gamma}{2c^2}\int_{-\infty}^{0}\tilde{\kappa}_{70}e^y\,dy$$
$$+\frac{1}{c}\int_{-\infty}^{0}\tilde{\kappa}_{50}e^y\,dy, \tag{A 15}$$

$$\kappa_{60} = \frac{1}{16(1-2\gamma)^2}\left[(1-2\gamma)^2\frac{\partial^4\psi^b}{\partial y^4}+12\gamma(1-2\gamma)\frac{\partial^3\psi^b}{\partial y^3}\right.$$
$$+(-28\gamma^2+16\gamma+8)\frac{\partial^2\psi^b}{\partial y^2}-48\gamma(1-2\gamma)\frac{\partial g_{00}}{\partial y}$$
$$\left.+2(-40\gamma^2+34\gamma+11)\frac{\partial g_{00}}{\partial y}\right]_{y=0}+\frac{1}{c}\int_{-\infty}^{0}\tilde{\kappa}_{60}e^y\,dy, \tag{A 16}$$

where the coefficients $\tilde{\kappa}_{30}$–$\tilde{\kappa}_{70}$ in the integrands are defined as

$$\tilde{\kappa}_{30} = -\frac{c}{4}\left[8g_{10}-4g_{00}+y^2e^y\frac{\partial^3\psi^b}{\partial y^3}+2e^y\left(\frac{\partial\psi^b}{\partial y}\right)_{y=0}\right], \tag{A 17}$$

$$\tilde{\kappa}_{40} = \frac{\partial^3\psi^b}{\partial y^3}\left[g_{20}+\frac{1}{c}g_{00}\frac{\partial\psi^b}{\partial y}-\frac{1}{2c}e^y\frac{\partial\psi^b}{\partial y}\left(\frac{\partial\psi^b}{\partial y}\right)_{y=0}+\frac{1}{2c}e^y\left(\frac{\partial\psi^b}{\partial y}\right)^2\right], \tag{A 18}$$

$$\tilde{\kappa}_{50} = -2cg_{20}-\frac{1}{2}\frac{\partial^3\psi^b}{\partial y^3}\left\{2g_{10}-2g_{00}-ye^y\frac{\partial\psi^b}{\partial y}+\left[\left(\frac{\partial\psi^b}{\partial y}\right)_{y=0}-\frac{\partial\psi^b}{\partial y}\right]e^y\right\}, \tag{A 19}$$

$$\tilde{\kappa}_{60} = -\frac{c}{16}e^{3y}\frac{\partial^5\psi^b}{\partial y^5}-\frac{c(2-\gamma)}{8(1-2\gamma)}e^{3y}\frac{\partial^4\psi^b}{\partial y^4}-\frac{c(8\gamma+5)}{16(1-2\gamma)}e^y\frac{\partial^3\psi^b}{\partial y^3}, \tag{A 20}$$

$$\tilde{\kappa}_{70} = \frac{1}{2c}\frac{\partial^3\psi^b}{\partial y^3}\left\{2g_{00}-\left[\left(\frac{\partial\psi^b}{\partial y}\right)_{y=0}-\frac{\partial\psi^b}{\partial y}\right]e^y\right\} \tag{A 21}$$

and the functions $g_{00}(y), g_{01}(y), g_{10}(y), g_{20}(y), g_{30}(y)$ satisfy the following governing equations:

$$\partial^2 g_{00}/\partial y^2 - g_{00} = -\tfrac{1}{2}\mathrm{e}^y \partial^3 \psi^b/\partial y^3, \tag{A 22}$$

$$\partial^2 g_{01}/\partial y^2 - g_{01} = -\tfrac{1}{2}\mathrm{e}^y \partial^3 \psi^q/\partial y^3, \tag{A 23}$$

$$\frac{\partial^2 g_{10}}{\partial y^2} - g_{10} = -2g_{00} + \left(\frac{\partial \psi^b}{\partial y}\right)_{y=0} \mathrm{e}^y + \tfrac{1}{2} y \mathrm{e}^y \frac{\partial^3 \psi^b}{\partial y^3}, \tag{A 24}$$

$$\frac{\partial^2 g_{20}}{\partial y^2} - g_{20} = -\frac{1}{c} g_{00} \frac{\partial^3 \psi^b}{\partial y^3} + \frac{1}{2c}\left[\left(\frac{\partial \psi^b}{\partial y}\right)_{y=0} - \frac{\partial \psi^b}{\partial y}\right] \mathrm{e}^y \frac{\partial^3 \psi^b}{\partial y^3}, \tag{A 25}$$

$$\frac{\partial^2 g_{30}}{\partial y^2} - 4g_{30} = \tfrac{1}{8}\mathrm{e}^{2y} \frac{\partial^4 \psi^b}{\partial y^4} - \frac{3\gamma}{4(1-2\gamma)} \mathrm{e}^{2y} \frac{\partial^3 \psi^b}{\partial y^3}, \tag{A 26}$$

with boundary conditions

$$g_{00} = g_{01} = g_{10} = g_{20} = g_{30} = 0, \quad y = 0, -\infty. \tag{A 27}$$

To obtain the modified mean current ψ^q we first write the apparent mean tangential stress as

$$2\epsilon c|A|^2 + q_0 = \epsilon\left[q'\left(x_1 - \frac{1+3\gamma}{2(\gamma+1)^{\frac{1}{2}}} t_1, x_2, x_3, \ldots, t_2, t_3, \ldots\right) + q(\tau)\right], \tag{A 28}$$

where ϵq is the average of the left-hand side over x_1 or t_1. Then the second derivative of ψ^q is solved to be

$$\frac{\partial^2 \psi^q}{\partial y^2} = \frac{-y}{2(N\epsilon\pi)^{\frac{1}{2}}} \int_0^\tau q(\tau - s) \frac{1}{s^{\frac{3}{2}}} \exp\left(-\frac{y^2}{4sN\epsilon}\right) \mathrm{d}s \tag{A 29}$$

and the first derivative is obtained by integrating (A 29) from $y = -\infty$ to $y = y$. Details are given in Hara & Mei (1991).

REFERENCES

BLENNERHASSETT, P. J. 1980 On the generation of waves by wind. *Phil. Trans. R. Soc. Lond.* A **298**, 451–494.

CAPONI, E. A., FORNBERG, B., KNIGHT, D. D., MCLEAN, J. W., SAFFMAN, P. G. & YUEN, H. C. 1982 Calculation of laminar viscous flow over a moving wavy surface. *J. Fluid Mech.* **124**, 347–362.

CHEN, B. & SAFFMAN, P. G. 1979 Steady gravity-capillary waves on deep water – I. Weakly nonlinear waves. *Stud. Appl. Maths* **60**, 183–210.

CHOI, I. 1977 Contributions a l'étudé des mecanismes physiques de la génération des ondes de capillarité-gravité à une interface air-eau. Thesis, Université d'Aix Marseille.

DJORDJEVIC, V. D. & REDEKOPP, L. G. 1977 On two dimensional packets of capillary–gravity waves. *J. Fluid Mech.* **79**, 703–714.

DYSTHE, K. B. 1979 Note on a modification to the nonlinear Schrödinger equation for application to deep water waves. *Proc. R. Soc. Lond.* A **369**, 105–114.

GASTEL, K. VAN, JANSSEN, P. A. E. M. & KOMEN, G. J. 1985 On phase velocity and growth rate of wind-induced gravity-capillary waves. *J. Fluid Mech.* **161**, 199–216.

HARA, T. 1990 Nonlinear dynamics near a wavy boundary on the sea surface or the sea bottom. PhD thesis, Dept. of Civil Engng, Massachusetts Institute of Technology.

HARA, T. & MEI, C. C. 1991 Frequency downshift in narrow-banded surface waves under the influence of wind. *J. Fluid Mech.* **230**, 429–477.

HOGAN, S. J. 1985 The fourth-order evolution equation for deep-water gravity–capillary waves. *Proc. R. Soc. Lond.* A **402**, 359–372.

JANSSEN, P. A. E. M. 1986 The periodic-doubling of gravity–capillary waves. *J. Fluid Mech.* **172**, 531–546.

KAWAI, S. 1979 Generation of initial wavelets by instability of a coupled shear flow and their evolution to wind waves. *J. Fluid Mech.* **93**, 661–703.

LAKE, B. M., YUEN, H. C., RUNGALDIER, H. & FERGUSON, I. N. E. 1977 Nonlinear deep water waves: theory and experiment. Part 2. Evolution of a continuous wave train. *J. Fluid Mech.* **83**, 49–74.

LARSON, T. R. & WRIGHT, J. W. 1975 Wind-generated gravity–capillary waves: laboratory measurements of temporal growth rates using microwave backscatter. *J. Fluid Mech.* **70**, 417–436.

LO, E. & MEI, C. C. 1985 A numerical study of water-wave modulation based on a higher-order nonlinear Schrödinger equation. *J. Fluid Mech.* **150**, 395–416.

MCGOLDRICK, L. F. 1965 Resonant interactions among capillary–gravity waves. *J. Fluid Mech.* **21**, 305–331.

MILES, J. W. 1957 On the generation of surface waves by shear flows. *J. Fluid Mech.* **3**, 185–204.

MILES, J. W. 1961 On the generation of surface waves by shear flows. Part 4. *J. Fluid Mech.* **13**, 433–448.

SCHLICHTING, H. 1955 *Boundary-Layer Theory*. McGraw-Hill.

TRULSEN, K. & DYSTHE, K. B. 1989 Frequency down-shift through self modulation and breaking. In *Water Wave Kinematics*, NATO ASI Series. Kluwer.

VALENZUELA, G. R. 1976 The growth of gravity–capillary waves in a coupled shear flow. *J. Fluid Mech.* **76**, 229–250.